

Gamma-ray lines and One-Loop Continuum from s -channel Dark Matter Annihilations

C. B. Jackson^a, Géraldine Servant^{b,c,d}, Gabe Shaughnessy^e,
Tim M.P. Tait^f, and Marco Taoso^{d,g}

^a*University of Texas at Arlington, Arlington, TX 76019 USA*

^b*CERN Physics Department, Theory Division, CH-1211 Geneva 23, Switzerland*

^c*ICREA at IFAE, Universitat Autònoma de Barcelona, 08193 Bellaterra, Barcelona, Spain*

^d*Institut de Physique Théorique, CEA/Saclay, F-91191 Gif-sur-Yvette Cédex, France*

^e*Department of Physics, University of Wisconsin, Madison, WI 53706 USA*

^f*Department of Physics & Astronomy, University of California, Irvine, CA 92697 USA*

^g*Department of Physics & Astronomy, University of British Columbia, Vancouver, BC V6T 1Z1 Canada*

geraldine.servant@cern.ch, chris@uta.edu,
gshau@hep.wisc.edu, ttait@uci.edu, marco.taoso@cea.fr

Abstract

The era of indirect detection searches for dark matter has begun, with the sensitivities of gamma-ray detectors now approaching the parameter space relevant for weakly interacting massive particles. In particular, gamma ray lines would be smoking gun signatures of dark matter annihilation, although they are typically suppressed compared to the continuum. In this paper, we pay particular attention to the 1-loop continuum generated together with the gamma-ray lines and investigate under which conditions a dark matter model can naturally lead to a line signal that is relatively enhanced. We study generic classes of models in which DM is a fermion that annihilates through an s -channel mediator which is either a vector or scalar and identify the coupling and mass conditions under which large line signals occur. We focus on the “forbidden channel mechanism” advocated a few years ago in the “Higgs in space” scenario for which tree level annihilation is kinematically forbidden today. Detailed calculations of all 1-loop annihilation channels are provided. We single out very simple models with a large line over continuum ratio and present general predictions for a large range of WIMP masses that are relevant not only for Fermi and Hess II but also for the next generation of telescopes such as CTA and Gamma-400. Constraints from the relic abundance, direct detection and collider bounds are also discussed.

1 Introduction

If dark matter (DM) is a thermally produced Weakly Interacting Massive Particle (WIMP), there is a lower bound on its total annihilation cross section to avoid overabundance of DM in the universe: independently of the details of thermal freeze-out and whether DM is “symmetric” or not, its thermally averaged annihilation cross section at the time of freeze-out $\langle\sigma v\rangle$ should be greater than order 1 pb $\sim 10^{-26}$ cm³/s. Assuming one saturates this bound (or in other words that the dark matter is a thermal relic), one can classify the prospects for the indirect detection of dark matter based on whether the annihilation is s -wave, $\langle\sigma v\rangle \propto 1$, or p -wave, $\langle\sigma v\rangle \propto v^2$, where v is the relative velocity of the annihilating particles. For a p -wave suppressed cross section, the prospects of experimentally observing annihilation products are poor, since v has fallen from $\mathcal{O}(1)$ at the time of freeze-out to $\sim 10^{-3}$ in our galaxy today. On the other hand, an s -wave annihilator has essentially the same $\langle\sigma v\rangle$ today as in the early universe, and indirect detection experiments are bearing down on the correct range. In fact, for WIMP masses below ~ 50 GeV, the thermal freeze-out cross section is narrowly excluded by null results from the Fermi LAT [1, 2].

In this work, we explore a class of models where annihilations in the early universe and annihilations today are controlled by different processes and thus are naturally of different sizes. Such a situation is motivated in models where the DM couples most significantly to particles with heavy masses. For instance, in scenarios of composite Higgs and top quarks, the new physics sector responsible for EW symmetry breaking only has sizable couplings with heavy states. If the DM is part of this sector, annihilation into light Standard Model (SM) states is often suppressed. If the mass difference between DM and the new heavy particles (which we generically denote as ψ) is less than a few tens of GeV, the DM kinetic energy in the early universe allows tree level annihilation into ψ pairs and the correct relic abundance can be obtained for couplings of order 1. On the other hand, in this “forbidden channel” scenario, tree level annihilation into ψ pairs is kinematically forbidden in the current epoch¹.

We proposed such a scenario a few years ago in the “Higgs in Space” model [3], which was inspired by models of (partial) compositeness where the top quark is the only SM particle with sizable couplings to the new physics sector [4–7]. In a simple realization we explored a Z' vector mediator which had large couplings to DM and to the top quark but suppressed couplings to the other SM particles. Thermal freeze-out in the early universe is controlled by DM annihilation into top pairs, and for DM masses slightly below the top mass (~ 150 GeV), one can obtain the correct relic abundance while having very suppressed annihilation into the three-body final state tWb in our galaxy. Annihilation can be dominated by one loop channels, and this scenario can naturally lead to large gamma ray line signatures relative to the continuum.

In this work, we consider a larger class of scenarios in the same category. In all of the theories, we assume the DM is a Dirac fermion whose primary interactions with the SM are through a scalar or vector s -channel mediator, leading to annihilations of the form shown in Fig. 1. While there has recently been considerable interest in similar theories [8], we flesh out the discussion in a number of important ways. In particular, we demonstrate that it is not sufficient to suppress tree level annihilations; one must also take a close look at the one-loop

¹ Another interesting aspect of this class of models is that direct detection constraints are often naturally eluded.

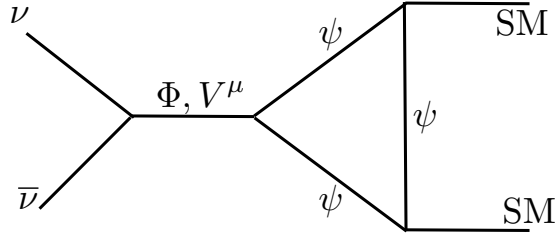


Figure 1: General topology studied in this paper. DM (ν) annihilates through an s -channel scalar Φ or vector V^μ resonance and loop of new fermions ψ .

contributions to the continuum gamma rays as well. We carry out a thorough investigation of this question by studying representative examples.

The plan is the following: in Section 2 we illustrate the idea with a very simple model where DM annihilates via a scalar Φ into a heavy fermion ψ . We explore different choices of couplings and gauge representations for ψ . We compute in detail all one-loop annihilation channels and determine the line-to-continuum ratio $\sigma_{\text{line}}/\sigma_{\text{continuum}}$, which characterizes the strength of the line signal relative to the DM-induced continuum background, and provides a useful analysis handle on any putative line signal [9]. Section 3 discusses the vector mediator case, distinguishing vector and axial couplings. If DM has axial couplings, both vector and scalar s -channel exchanges can play an important role. We compute all one-loop contributions to the continuum for various assumptions on the nature of the couplings (scalar, pseudoscalar, vector, axial). We summarize our conclusions in Section 4. In the appendices, we collect the expressions describing all of the one-loop annihilation processes. These results go somewhat beyond the immediate needs of the current work, and are easily adapted to any WIMP model whose interactions with the SM are primarily through an s -channel mediator.

2 Scalar Mediator Model

As a first example illustrating the forbidden channel scenario, we consider a model with a minimal dark sector: in addition to the (SM singlet) Dirac fermion DM, ν , we include another Dirac fermion ψ with vector-like SM gauge interactions which acts as the portal to the SM. ν and ψ can interact by exchanging a real scalar singlet Φ . We will eventually consider various possibilities for the gauge quantum numbers of ψ , but begin by assuming that it is a color singlet and a doublet under $SU(2)$ carrying the opposite hypercharge $Y = 1/2$ to the SM lepton doublet. In that case, the relevant interactions are given by

$$\mathcal{L} \supset -\bar{\nu}(y_{\nu\Phi}^S + iy_{\nu\Phi}^P\gamma^5)\nu\Phi - \bar{\psi}(y_{\psi\Phi}^S + iy_{\psi\Phi}^P\gamma^5)\psi\Phi - y_H \bar{\psi}H\nu + h.c \quad (1)$$

where H is the SM Higgs doublet and we have assumed as usual that a dark symmetry (parity or $U(1)_D$) forbids ν from mixing with the SM neutrinos via interactions such as $LH\nu$. The last term is responsible for the decay of $\psi \rightarrow h\nu$ (where h is the SM Higgs boson), with y_H chosen to be smaller than $\sim 10^{-3}$ to avoid a degree of $\psi^0 - \nu$ mixing which induces a dangerous Z - ν - $\bar{\nu}$ coupling excluded by direct DM searches, but large enough for

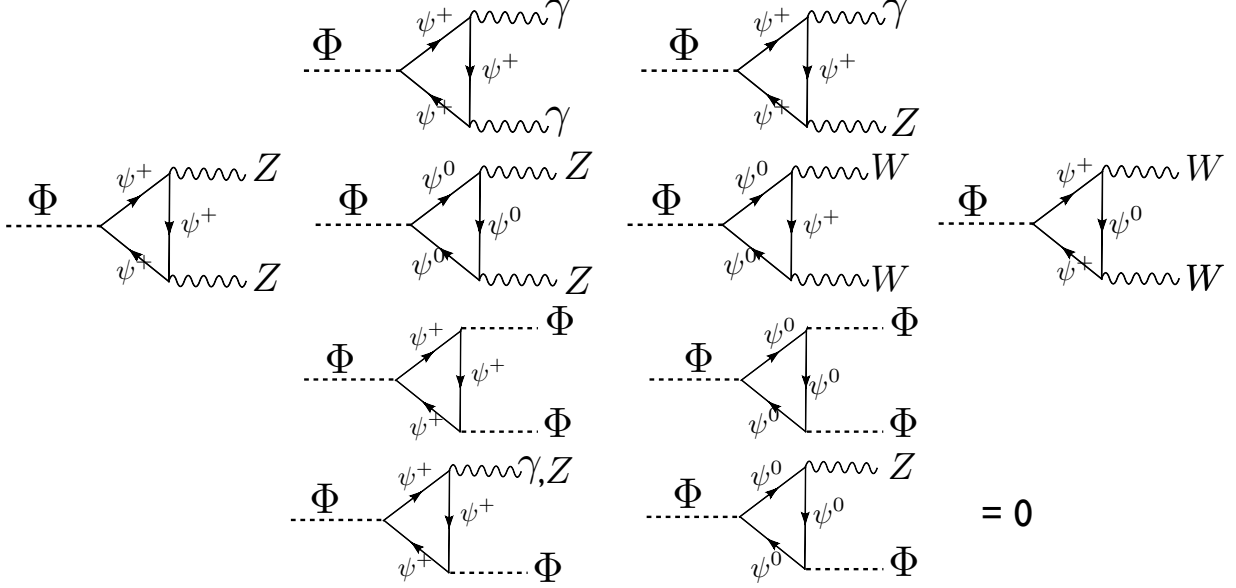


Figure 2: Representative Feynman diagrams for relevant one loop processes in the scalar model with an $SU(2)$ doublet ψ with $Y = 1/2$. The last two diagrams, corresponding to annihilation into $\gamma\Phi$ and $Z\Phi$, vanish due to angular momentum and CP conservation respectively.

ψ to decay before BBN. For this range of values, it is safely small enough as to be roughly irrelevant for the remainder of our discussion.

In addition, there are interactions such as $|H|^2\Phi$ which after electroweak breaking induce mixing between Φ and the SM Higgs. We characterize the degree of mixing as $\sin\alpha$, with the unmixed limit obtained as $\sin\alpha \rightarrow 0$. A small amount of such mixing is welcome to allow Φ to decay, and as we shall see below can help arrange for the correct ν relic density, but a large degree of mixing would lead to a large direct detection rate which could be problematic. We will discuss ranges of $\sin\alpha$ together with the relic density in more detail, below.

The one-loop annihilation channels mediated by Φ are shown in Fig. 2, including potentially three lines (corresponding to $\gamma\gamma$, γZ , and $\gamma\Phi$) at distinct energies². However, in practice the $\gamma\Phi$ (and $Z\Phi$) channels mediated by an s -channel scalar vanish because they do not conserve angular momentum or CP. All of the corresponding cross sections scale as

$$\langle\sigma v\rangle \propto ((y_{\nu\Phi}^S)^2 v^2 + 4(y_{\nu\Phi}^P)^2) \quad (2)$$

which in the non-relativistic limit is p -wave suppressed for purely scalar couplings. We therefore concentrate on pseudo-scalar couplings of Φ to DM to be able to observe a sizable γ -ray line signal (in which case the elastic scattering via Higgs exchange after $h - \Phi$ mixing is velocity suppressed). On the other hand, large line signals are not predicated on the nature of the $\Phi - \psi$ coupling. Detailed expressions in the $v \rightarrow 0$ limit are given in the appendices. In addition, the final states consisting of a vector and a scalar particle vanish for the s -channel

²The presence of a forest of multiple lines is a generic feature arising from $SU(2) \times U(1)$ gauge invariance [10, 11].

$y_{\psi\Phi}$	S	P
$\gamma\gamma$	✓	✓
γZ	✓	✓
$\gamma\Phi$	0	0
$Z\Phi$	0	0
$\Phi\Phi$	✓	0
ZZ	✓	✓
WW	✓	✓

	ψ_{-1}	$\psi_{-3/2}$	$\psi_{1/2}$
$\sigma_{\gamma Z}/\sigma_{cont}$	10	0.5	0.02
$\sigma_{\gamma\gamma}/\sigma_{cont}$	30	1	0.04

Table 1: Summary of the one-loop DM annihilation channels in scalar exchange models and typical (but parameter-dependent) values of the line/continuum ratio for the three charge assignments discussed in the text. σ_{cont} is the sum of all the 1-loop continuum cross sections.

scalar exchange. A summary of the various channels for the scalar (S) and pseudo-scalar (P) $\Phi - \psi$ couplings is shown in Table 1. It is worth noting that the t -channel tree level annihilation into $\Phi\Phi$ is p -wave suppressed in all cases, and therefore annihilation into $\Phi\Phi$ is controlled by the one-loop contribution.

As alluded to above, there is a wider variety of SM $SU(2) \times U(1)$ gauge charges for ψ which can result in a viable line signal. We study the particular cases of SM representations ($SU(3)$, $SU(2)$, $U(1)$):

- (1, 2, 1/2): $\psi_{1/2} = (\psi^+, \psi^0)$;
- (1, 2, -3/2): $\psi_{-3/2} = (\psi^-, \psi^{--})$;
- (1, 1, -1): $\psi_{-1} = \psi^-$.

In terms of the dark symmetry, in the case $\psi = \psi_{1/2}$, ψ is charged under the dark symmetry as well and decays into νH ; when $\psi = \psi_{-3/2}$, ψ is uncharged and can decay into He_R ; and when $\psi = \psi_{-1}$, we also assume it is uncharged and decays into SM states via a tiny mixing with the SM right-handed lepton (note that the last term in Eq. (1) is only present for $\psi = \psi_{1/2}$). In all cases, these couplings allowing ψ to decay can be chosen small enough that they do not play much role in dark matter searches or in determining the relic density.

In Figures 3 and 4, we show the (complete one loop) cross sections for the cases where ψ has scalar (dotted) or pseudo scalar (solid) coupling. We illustrate the resonant dependence on M_Φ for fixed DM mass, the dependence on M_ψ , the line cross section to continuum cross section, $\sigma_{line}/\sigma_{continuum}$, and contours of fixed cross sections the M_ν - M_Φ parameter plane. For $\psi = \psi_{1/2}$, the WW cross section is large relative to the $\gamma\gamma$ or γZ channels and the line to continuum ratio $\sigma_{line}/\sigma_{continuum}$ is typically around 0.02 to 0.04 (still larger than what a random WIMP model with tree level annihilation would predict [9]). Much larger ratios can be obtained for the two other cases. For $\psi = \psi_{-3/2}$, the ratio goes up to ~ 1 , with both ψ^- and ψ^{--} contributing to the line signal. When ψ is an $SU(2)$ singlet, $\psi = \psi_{-1}$, there is no annihilation into WW , with the line to continuum ratio jumping to values as large as ~ 30 . We illustrate the spectrum of a few promising cases in Figure 5.

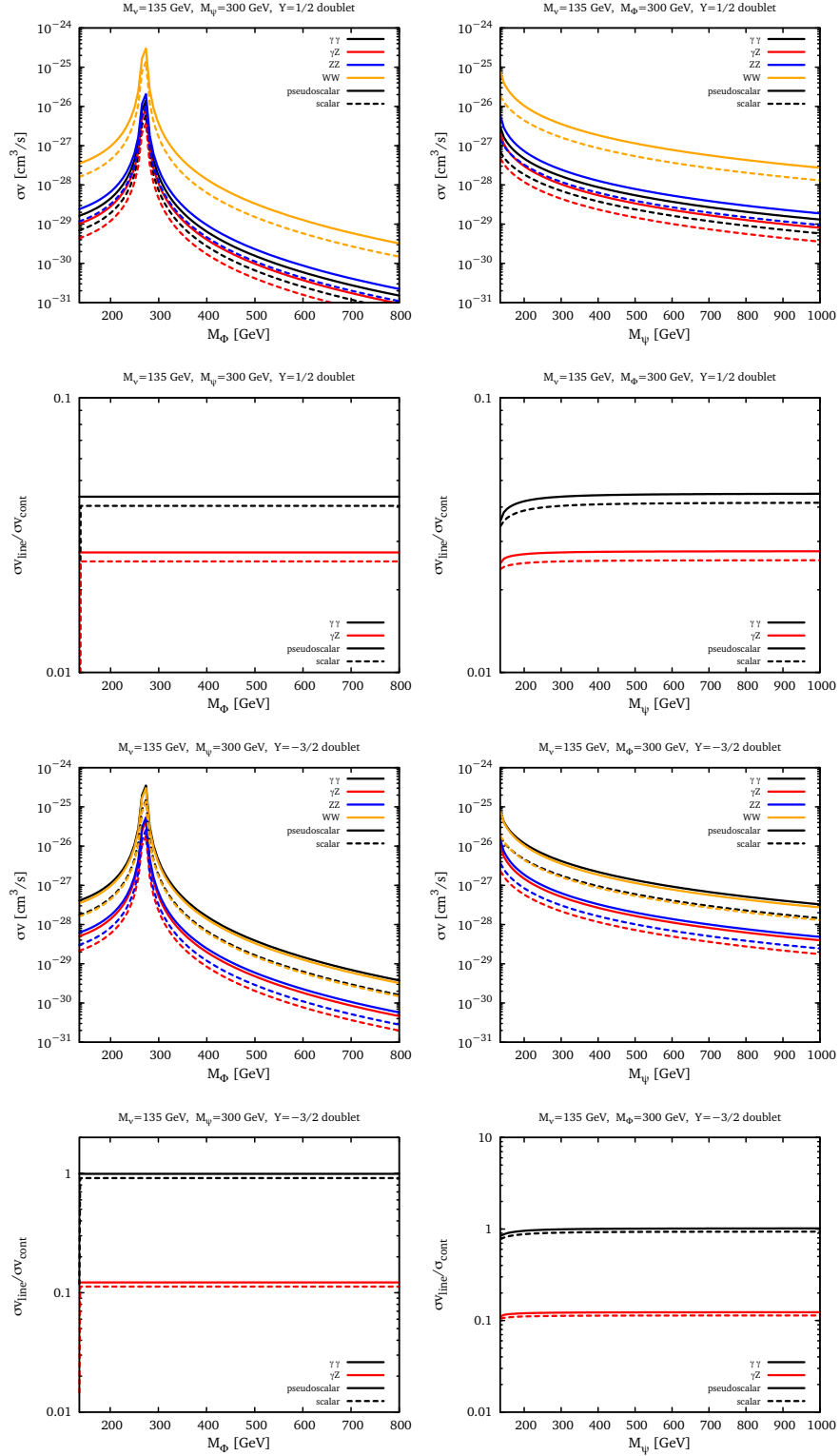


Figure 3: Gamma ray line signal and continuum strength for scalar exchange models: top: the (1, 2, 1/2) case; bottom: the (1, 2, -3/2) case.

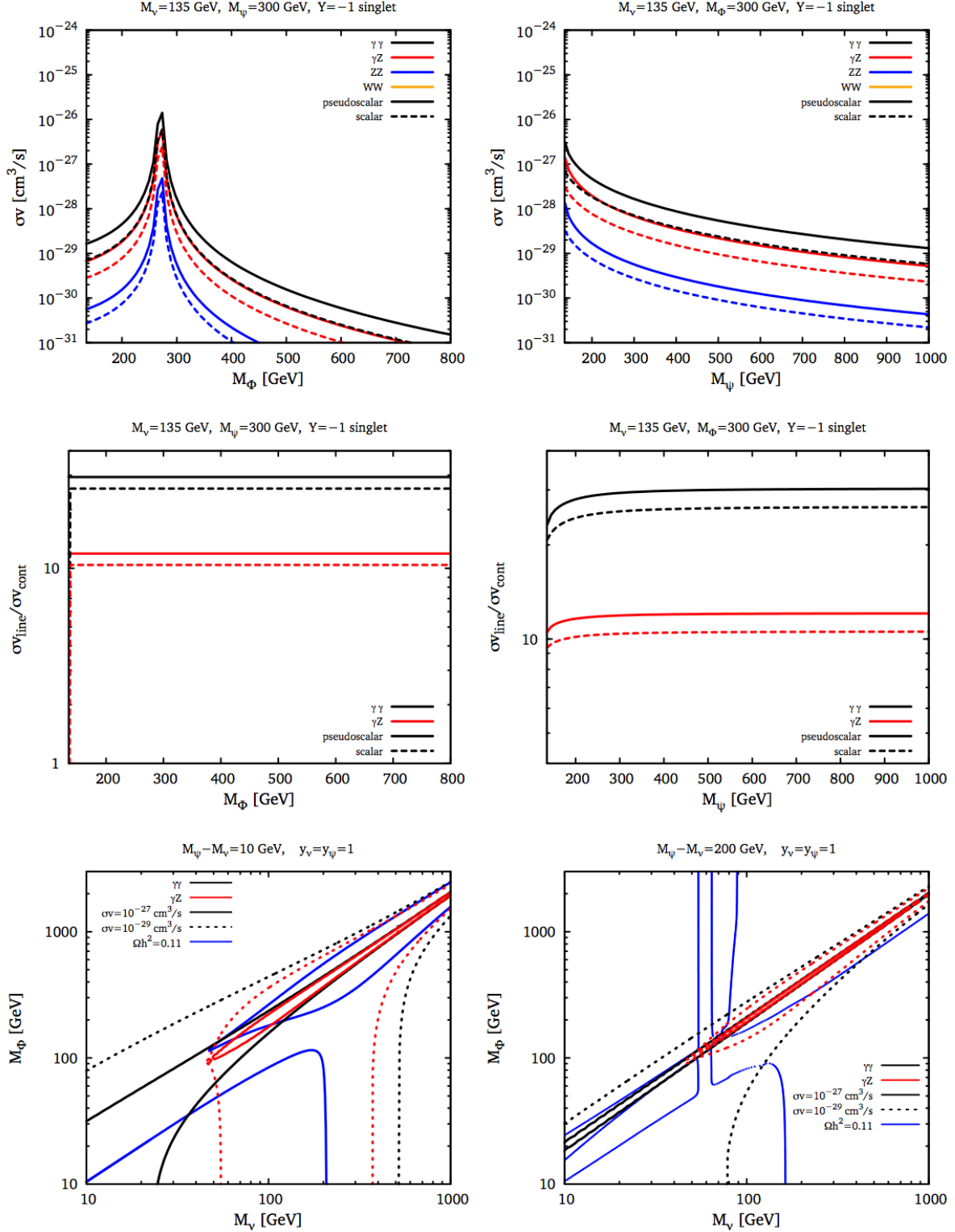


Figure 4: Gamma ray line signal and continuum strength for scalar exchange models in the (1, 1, -1) case. In the last two plots, we added the contours corresponding to correct relic abundance.

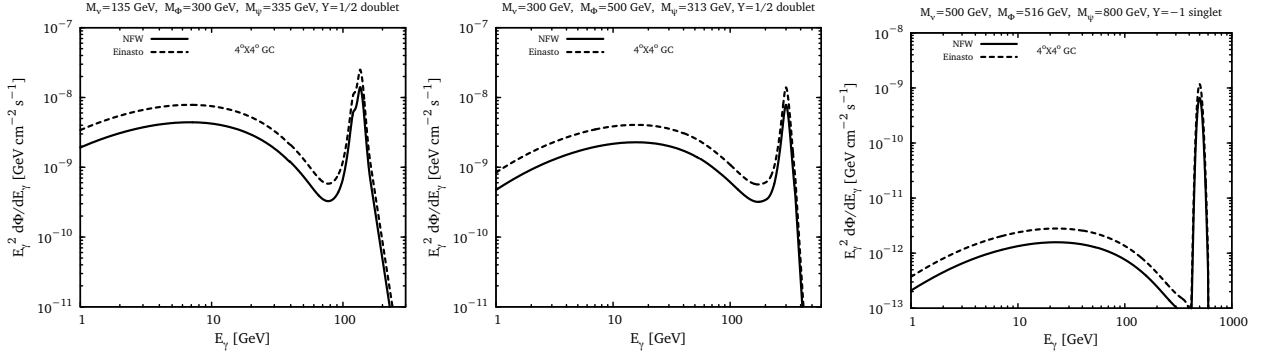


Figure 5: Examples gamma-ray spectra for three choices of parameters leading to the correct DM relic abundance and for two choices of DM profiles.

Since all of the channels experience the same resonant enhancement, the ratios do not depend on M_Φ (though as shown, together with the DM mass, it does control the absolute values of the cross sections). Increasing M_ψ leads to the fall-off in the absolute rates shown on the figures. We have fixed the DM mass to 135 GeV for illustration, inspired by the features in the Fermi LAT data from the galactic center [11–13]; the values of the ratios are not very sensitive to this choice of mass and one can easily realize strong lines at other energies.

This class of models provides simple examples of potentially large gamma ray line signatures. It is also easy to obtain the correct relic abundance in this setup. For non-zero $\sin \alpha$, the h - Φ mixing produces resonant enhancement of the annihilation cross section for $M_\nu \simeq M_h/2 \simeq 62$ GeV, and for $M_\nu \simeq M_\Phi/2$. The width of Φ and its coupling to SM final states are both controlled by $\sin \alpha$. The resulting relic density is a complicated function of the DM mass, as illustrated in Fig. 6. Typically, there will be regions around both the h and Φ resonances with the correct relic abundance. Obviously, the regions around the Φ resonance will also lead to large gamma ray line features. Since the ψ mass is slightly above the DM mass, one could also invoke coannihilation between ν and ψ . Similarly, when ψ decays into SM states and it is slightly heavier than ν , $\nu\bar{\nu} \rightarrow \psi\bar{\psi}$ annihilations are efficient in the early universe, although forbidden today. This is the forbidden channel idea proposed in [3], where the role of ψ was played by the top quark. While it is generically true that one can arrange for both large gamma ray line signals and the correct relic density, there is no firm generic correlation between the two processes.

We close this section with some brief discussion of collider and precision measurements. Since all choices of ψ are vector-like, with at most extremely tiny mixing with SM fermions, constraints to precision electroweak observables [14] are expected to be much weaker than direct constraints from colliders. Since the ψ states contain charged particles which can decay into leptons, low-background final states at the LHC are possible; however, these are balanced by very small electroweak production cross sections. As a result, current experimental constraints are rather weak, and new states as light as a few hundreds of GeV are allowed. We expect that further high energy running of the LHC should eventually cover a good portion of the parameter space.

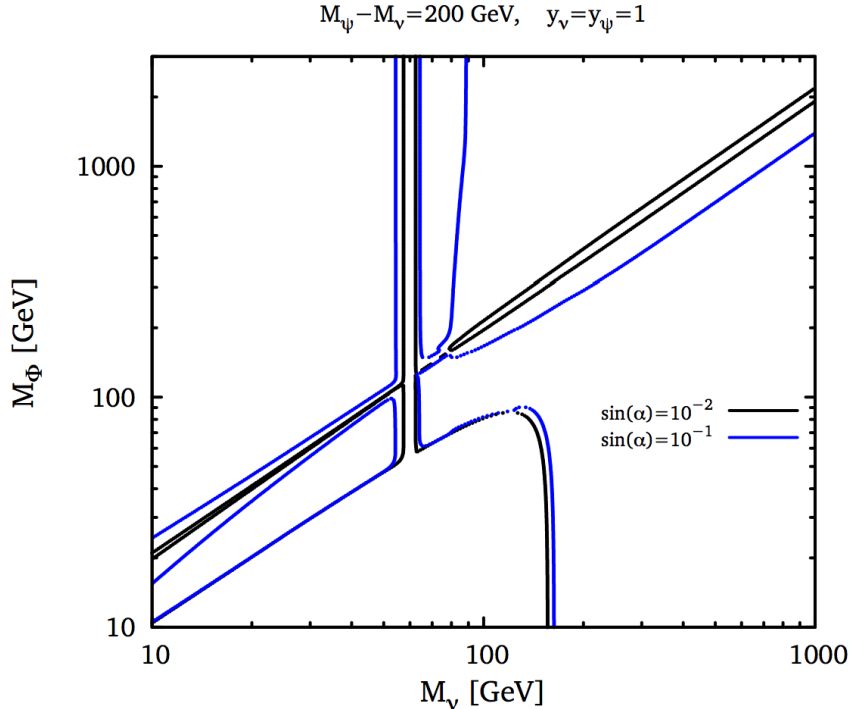


Figure 6: Contours of correct relic abundance in the M_ν - M_Φ plane from annihilations into $\psi\psi$ and $\Phi\Phi$ (where allowed) and SM states via $h - \Phi$ mixing.

3 Vector Mediator Model

The case of an s -channel vector mediator builds on what we have learned from the scalar model in the previous section. The SM gauge sector is extended by a $U(1)'$ gauge symmetry which is broken by the VEV of a complex scalar, resulting in a spectrum consisting of a massive vector boson Z' and the associated Higgs scalar Φ . Their masses can be related to the $U(1)'$ -breaking VEV,

$$M_{Z'} = g_{Z'} q_\Phi \langle \Phi \rangle, \quad (3)$$

$$M_\Phi = \sqrt{a} \langle \Phi \rangle. \quad (4)$$

where q_Φ is the charge of the complex scalar, $g_{Z'}$ is the $U(1)'$ gauge coupling, and a is the scalar quartic, which we will fix to 1 to illustrate the typical physics. The phenomenology associated with Φ exchange is very similar to the scalar model of the previous section, including the possibility that it mixes with the SM Higgs h through couplings such as $|H|^2|\Phi|^2$.

The DM is charged under $U(1)'$, as are the ψ fermions. As in the case of the scalar exchange models, there are a variety of viable choices for the representations of ψ under the SM. In practice, we choose ψ to be an $SU(2)$ singlet carrying one unit of hypercharge. In principle, nothing determines the $SU(3)$ representation of ψ ; in practice we choose them to be uncolored in order to evade large annihilation into gg [15, 16] as well as the LHC bound on t' -like objects of about 450 GeV [17, 18]. We leave the case where ψ is colored (and can mix) with the right-handed top quark for separate work [19].

Any additional $U(1)'$ symmetry will generally kinetically mix with the SM hyper-charge boson. This mixing is a free parameter of the theory, and is additively renormalized by loops of the ψ fields. In order not to induce a large contribution to direct scattering, the mixing parameter should be smaller than of order 10^{-3} , consistent with a value induced by loop processes without any large cancellations [19].

3.1 Mass Structure versus Couplings

We will find that the one-loop cross sections in this setup are very sensitive to the vector or axial nature of the couplings, as summarized in Table 2. If all couplings in the loop are vector-like, there is no one-loop annihilation into two gauge bosons. In practice, an odd number of axial vector couplings is required in the loop for the annihilation cross section to survive in the non-relativistic limit. To avoid SM anomalies, we take ψ to have vector-like couplings with respect to the SM gauge group, therefore, strong line signals require axial vector couplings of the Z' to ν or ψ (or both). This implies that both states are actually hybrids of underlying states with different $U(1)'$ charges, married together by $\langle\Phi\rangle$.

In order to avoid mixed $U(1)'$ -SM anomalies, we engineer this by including vector-like *pairs* of ν with charges q_{ν_1} and $q_{\nu_2} = q_{\nu_1} - q_\Phi$ and another vector-like pair of ψ fields with charges q_{ψ_1} and $q_{\psi_2} = q_{\psi_1} - q_\Phi$. In principle, the right- and left-chiral members of each pair could be married by a vector-like mass term, but we neglect these terms, which would induce dependence on a mixing angle, for simplicity³.

These charge assignments insure that Yukawa interactions with Φ are allowed, and after obtaining a VEV, result in mass terms for the two states in each pair,

$$M_\psi = \lambda_\psi^S \langle\Phi\rangle \quad , \quad M_{\psi'} = \lambda_{\psi'}^S \langle\Phi\rangle, \quad (5)$$

$$M_\nu = \lambda_\nu^S \langle\Phi\rangle \quad , \quad M_{\nu'} = \lambda_{\nu'}^S \langle\Phi\rangle. \quad (6)$$

where $\psi_R \equiv \psi_{2R}$, $\psi_L \equiv \psi_{1L}$, $\psi'_R \equiv \psi_{1R}$ and $\psi'_L \equiv \psi_{2L}$. These masses are bounded by perturbativity of the couplings to be less than about $\lesssim 4\pi\langle\Phi\rangle$.

This construction guarantees the presence of an axial-vector interaction. For models with purely vector-like interactions, we can choose $q_{\nu_1} = q_{\nu_2}$ and $q_{\psi_1} = q_{\psi_2}$, which forbids interactions with Φ , but allows us to write down a gauge invariant mass for the field of interest. In that case, the heavier element of the pair is superfluous.

The most important terms in the Lagrangian read:

$$\begin{aligned} \mathcal{L} \supset & i \bar{\nu}_1 \not{D} \nu_1 + i \bar{\nu}_2 \not{D} \nu_2 + i \bar{\psi}_1 \not{D} \psi_1 + i \bar{\psi}_2 \not{D} \psi_2 \\ & - (\bar{\nu}_1 (y_{\nu\Phi}^S + i y_{\nu\Phi}^P \gamma^5) \nu_2 \Phi + h.c) - (\bar{\psi}_1 (y_{\psi\Phi}^S + i y_{\psi\Phi}^P \gamma^5) \psi_2 \Phi + h.c) , \end{aligned} \quad (7)$$

where

$$D_\mu \nu = \partial_\mu \nu - i g_{Z'} q_\nu Z'_\mu \nu , \quad (8)$$

$$D_\mu \psi = \partial_\mu \psi - i g_{Z'} q_\psi Z'_\mu \psi - i g_Z Z_\mu \psi - i Q_e^\psi e A_\mu \psi , \quad (9)$$

³As such terms are technically natural, there is no fine-tuning associated with this choice.

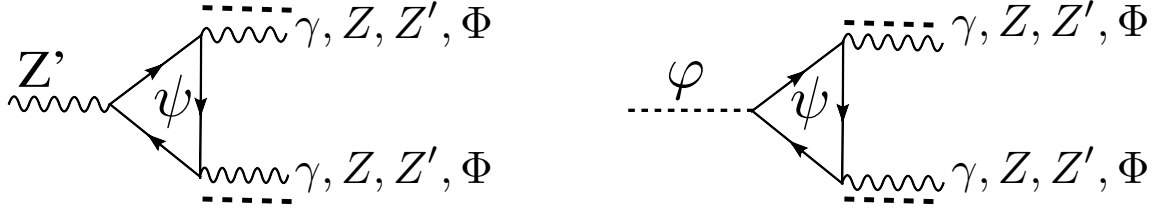


Figure 7: Representative one-loop annihilation channels in the vector model. The status of each channel depending on the nature of the couplings is summarized in Table 2.

for each $\nu_{1,2}$ and $\psi_{1,2}$, resulting in equal vector couplings and opposite axial-vector couplings of the mass eigenstates ψ and ψ' to Z' as:

$$\mathcal{L} \supset g_{Z'}(q_{\psi_1} - \frac{q_{\Phi}}{2})\bar{\psi}\gamma^{\mu}Z'_{\mu}\psi - \frac{g_{Z'}}{2}\bar{\psi}\gamma^{\mu}\gamma^5Z'_{\mu}\psi \quad (10)$$

$$+ g_{Z'}(q_{\psi_1} - \frac{q_{\Phi}}{2})\bar{\psi}'\gamma^{\mu}Z'_{\mu}\psi' + \frac{g_{Z'}}{2}\bar{\psi}'\gamma^{\mu}\gamma^5Z'_{\mu}\psi' \quad (11)$$

This module allows for tree level annihilation into $Z'Z'$, $Z'\Phi$ and $\psi\bar{\psi}$, all of which would lead to a large gamma-ray continuum. These potentially over-whelming contributions may be suppressed by imposing $M_{\nu} < M_{Z'}$ (i.e. $\lambda_{\nu}^S < g_{Z'}q_{\Phi}$), $M_{\nu} < (M_{\Phi} + M_{Z'})/2$, and $\lambda_{\nu}^S < \lambda_{\psi}^S$. Annihilation into $\Phi\Phi$ is p -wave suppressed, and thus there is no particular need to impose a relation between M_{ν} and M_{Φ} .

Representative one-loop annihilation diagrams are shown in Fig. 7. For a vector s -channel mediator, the $\gamma\gamma$ annihilation channel is non-zero only if DM has axial couplings (in which case Φ -mediated diagrams also contribute; see the appendices for details). This is one place in which our extended framework captures physics beyond what was studied in Ref. [3], where the DM was assumed to have vector-like couplings, and the $\gamma\gamma$ channel vanished. In addition, there are potentially gamma-ray line signals at various energies from annihilation into γZ , $\gamma Z'$ and/or $\gamma\Phi$. The $V\Phi$ final states proceed via s -channel vector exchange.

We classify different scenarios based on whether interactions of ν and ψ with the Z' are vector-like (V), axial-vector (A), or both (V+A). The various annihilation channels are listed along with their velocity-dependence, in Table 2. To recap the generic features:

- One-loop annihilations mediated by an s -channel scalar require pseudoscalar couplings of the DM.
- One-loop annihilations into $\gamma\gamma$ mediated by an s -channel vector are possible only for axial couplings of both the DM and ψ .
- One-loop annihilations into $\Phi\Phi$ require s -channel scalar exchange with pseudoscalar coupling of DM and scalar coupling of ψ .
- The γV channel mediated by an s -channel scalar requires vector coupling of ψ to V .
- The $\gamma\Phi$ channel requires vector couplings of both ν and ψ to the Z' .

	$g_{\nu Z'} = g_{\nu Z'}^V$						$g_{\nu Z'} = g_{\nu Z'}^A$				$g_{\nu Z'} = g_{\nu Z'}^V + g_{\nu Z'}^A$		
$g_{\psi Z}$	V	V	V	A	V+A	V+A	V	V	V	V+A	V	V	V
$g_{\psi Z'}$	V	A	V+A	V	V	V+A	V	A	V+A	V+A	V	A	V+A
$\gamma\gamma$	0	0	0	0	0	0	0	✓	✓	✓	0	✓	✓
γZ	0	✓	✓	✓	✓	✓	0	✓	✓	✓	0	✓	✓
$\gamma Z'$	0	0	✓	0	0	✓	0	0	✓	✓	0	0	✓
$\gamma\Phi$	0	0	✓	0	0	✓	0	0	0	0	0	0	✓
ZZ	0	✓	✓	0	✓	✓	0	✓	✓	✓	0	✓	✓
ZZ'	0	0	✓	✓	✓	✓	0	0	✓	✓	0	0	✓
$Z\Phi$	0	✓	✓	0	0	✓	0	✓	✓	✓	0	✓	✓
$Z'\Phi$	0	✓	✓	0	0	✓	0	0	✓	✓	0	✓	✓
$\Phi\Phi$	0	0	0	0	0	0	0	✓	✓	✓	0	✓	✓
$Z'Z'$	0	✓	✓	0	0	✓	0	✓	✓	✓	0	✓	✓

Table 2: One-loop DM annihilation channels in $U(1)'$ model due to a single fermion ψ running in the loop, where ψ carries hypercharge 1 but is $SU(2)$ singlet, for different combinations of vector (V) and axial (A) couplings. Unlisted combinations lead to vanishing cross sections in the non-relativistic limit.

The table displays the one-loop annihilation into $Z'Z'$ due to the ψ loops. However, while we have explicitly constructed a theory that is free of SM or mixed $U(1)'$ -SM anomalies, we have not been careful to impose cancellation of the $U(1)'^3$ anomaly. Cancellation of such anomalies will generically require the addition of fermions charged under $U(1)'$ (but not the SM), and thus the rate into $Z'Z'$ is somewhat more sensitive to the details of the UV completion. Besides, this one-loop channel, as well as $Z'\Phi$ and $\Phi\Phi$, requires additional box diagrams that are not considered in this work. We will always work in the kinematical regime where this channel is absent.

3.2 Vector DM Couplings

When the dark matter has vector-like coupling to the Z' , a strong line signal requires that ψ have axial-vector, or a combination of vector and axial vector couplings. In this case, there are three distinct lines: γZ , $\gamma Z'$, and $\gamma\Phi$. We illustrate this case in Fig. 8 for different configurations of parameters. Typically, the $\gamma Z'$ and $\gamma\Phi$ cross sections are much larger than γZ , with the $\gamma\Phi$ line very large for a wide range of Z' masses.

We show two representative gamma ray spectra in Fig. 9 obtained for $M_\nu = 300$ GeV. In the first plot, there are two close-by lines, one at an energy of $E_\gamma = 180$ GeV from $\gamma Z'$ ($\sigma_{\gamma Z'} v = 4.7 \times 10^{-29} \text{ cm}^3 \text{ s}^{-1}$), and one from $\gamma\Phi$ at $E_\gamma = 223$ GeV with $\sigma_{\gamma\Phi} v = 1.5 \times 10^{-28} \text{ cm}^3 \text{ s}^{-1}$. The continuum is rather suppressed and dominated by $Z\Phi$ annihilation with $\sigma v = 8 \times 10^{-28} \text{ cm}^3 \text{ s}^{-1}$. In the second plot, the mass of Z' is too large for the $\gamma Z'$ line to be observable ($\sigma_{\gamma Z'} v = 1.1 \times 10^{-33} \text{ cm}^3 \text{ s}^{-1}$) but there is a striking line at $E_\gamma = 135$ GeV and with $\sigma_{\gamma\Phi} v = 7.4 \times 10^{-29} \text{ cm}^3 \text{ s}^{-1}$. The continuum dominated by the $Z\Phi$ channel has

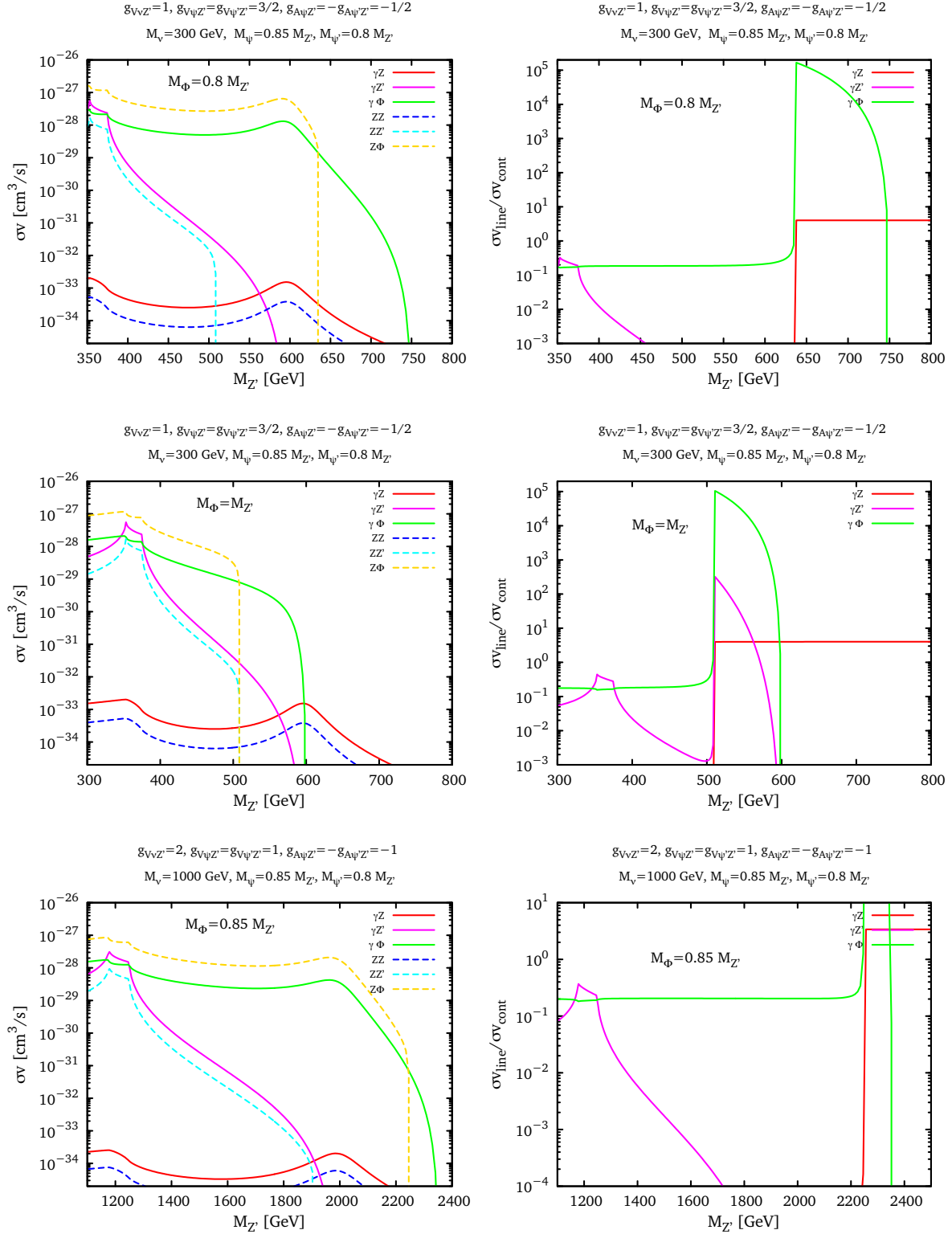


Figure 8: One-loop annihilation cross sections and ratio to continuum for DM with vector couplings, for a variety of parameter choices as indicated.

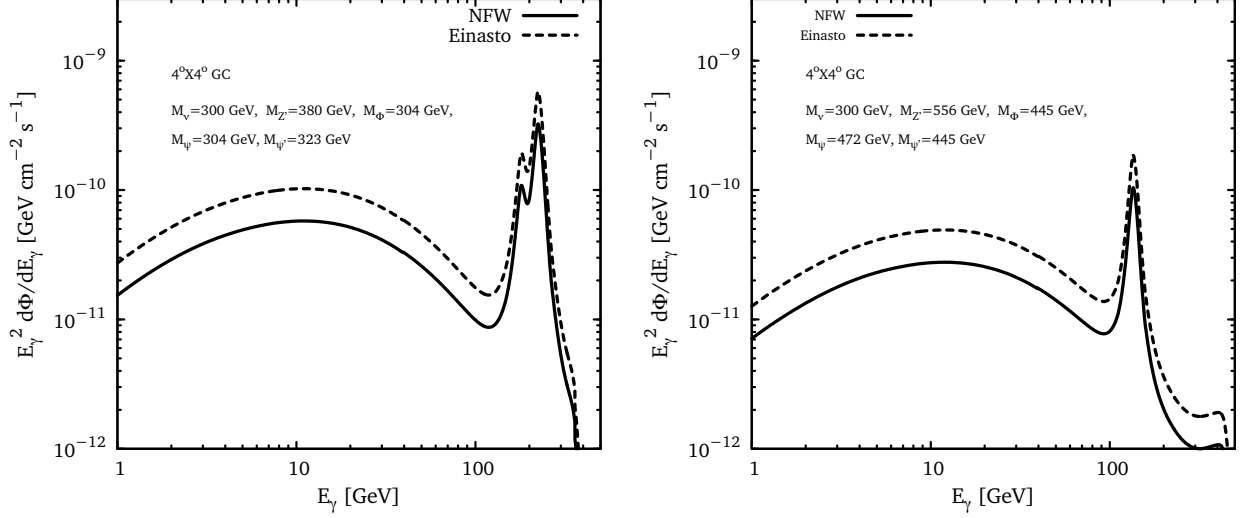


Figure 9: Gamma-ray spectrum obtained from $\nu\bar{\nu}$ annihilation in the galactic center with $M_\nu = 300$ GeV and other parameters as indicated.

$$\sigma_{Z\Phi} v = 3.9 \times 10^{-28} \text{ cm}^3 \text{ s}^{-1}.$$

3.3 Axial-Vector DM Couplings

When the DM has Z' axial vector couplings, it opens the door for the $\gamma\gamma$ channel and in addition there are contributions from Φ exchange to the annihilation channels. We illustrate this case in Figures 10, where we have chosen to switch off the pseudo-scalar coupling of the DM, and thus all diagrams mediated by s -channel scalar exchange vanish.

In Figure 10, we show the dependence of the cross sections on $M_{Z'}$, M_ν , and M_ψ . Because all three of these parameters are proportional to $\langle\Phi\rangle$, we vary them in a controlled way, exploring successively the variation with changing $\langle\Phi\rangle$ and all couplings fixed, variation of M_ν obtained by varying $y_{\nu\Phi}^S$ with all other parameters fixed, and variation of M_ψ obtained by varying $y_{\psi\Phi}^S$ with all other parameters fixed. From the figures, we see that either the $\gamma\gamma$ or $\gamma\Phi$ may end up as the strongest of the line signals (with $\gamma\gamma$ vanishing when the Z' goes on-shell, as required by the Landau-Yang theorem [20]), whereas the one loop continuum is rather anemic and is almost entirely made up of the $Z\Phi$ channel.

We show a representative two-peak gamma ray spectrum in Figure 11 for a case with $M_\nu = 330$ GeV. For these parameters, the $\gamma Z'$ line is somewhat too faint to be observed compared to the $Z\Phi$ continuum ($\sigma_{\gamma Z'} v = 1 \times 10^{-29} \text{ cm}^3 \text{ s}^{-1}$ and $\sigma_{Z\Phi} v = 4.5 \times 10^{-27} \text{ cm}^3 \text{ s}^{-1}$), but there are two large lines from the $\gamma\Phi$ and $\gamma\gamma$ channels at energies of $E_\gamma = 155$ and 330 GeV, respectively, with cross sections $\sigma_{\gamma\Phi} v = 8.5 \times 10^{-28} \text{ cm}^3 \text{ s}^{-1}$ and $\sigma_{\gamma\gamma} v = 1.2 \times 10^{-28} \text{ cm}^3 \text{ s}^{-1}$.

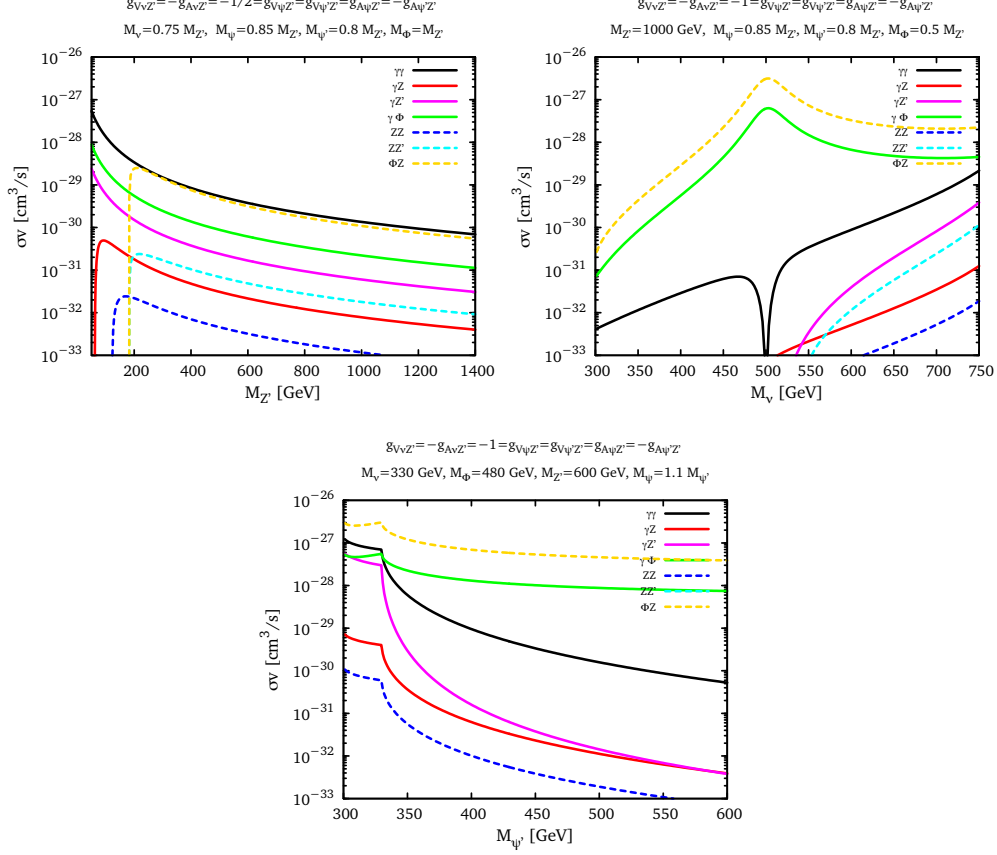


Figure 10: Cross sections for models where the DM has axial vector couplings, as a function of: a) $\langle\Phi\rangle$ (with all couplings held fixed); b) $y_{\nu\Phi}^S/M_\nu$ (with all other parameters held fixed); c) $y_{\psi\Phi}^S/M_\psi$ (with all other parameters held fixed).

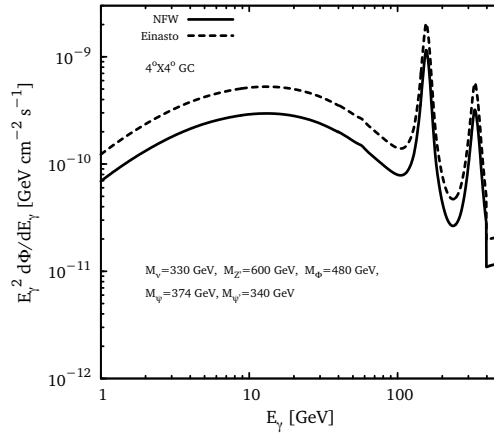


Figure 11: Two-peak Gamma-ray spectrum obtained from $\nu\bar{\nu}$ annihilation in the galactic center with $M_\nu = 330$ GeV and other parameters as shown.

3.4 A Purely Vector-Like Model

There is one further ingredient that is worthwhile to consider adding on top of the minimal framework we have introduced so far. In theories where the ν and ψ fields are composites, the most natural situation is one with only vector-like couplings. As shown in Table 2, this is not expected to lead to any observable line signals. However, such models often also predict additional scalars which are unrelated to the $U(1)'$ breaking, and are singlets under the SM, but have scalar interactions with the ψ fields. For example, composite Higgs models based on the $SO(6) \rightarrow SO(5)$ symmetry-breaking contain such a state S [22, 21]. Such an additional state opens up the possibility of strong gamma ray lines from the γS channel mediate by Z' exchange. In addition, one would also expect annihilation into ZS and $Z'S$. In order to simplify the discussion, we assume that the DM coupling to S is scalar, and thus any additional mediation via S itself vanishes in the non-relativistic limit. This case is summarized in Table 3 and illustrated with some representative quantitative results in Figure 12.

λ_ψ	λ_ν : scalar		λ_ν : pseudoscalar	
	scalar	pseudoscalar	scalar	pseudoscalar
$\gamma\gamma$	0	0	✓	✓
γZ	0	0	✓	✓
$\gamma Z'$	0	0	✓	✓
γS	✓	✓	✓	✓
ZZ	0	0	✓	✓
ZZ'	0	0	✓	✓
ZS	✓	0	✓	0
$Z'S$	✓	0	✓	0
SS	✓	0	✓	0
$Z'Z'$	0	0	✓	✓

Table 3: One-loop DM annihilation channels in the purely vector-like $U(1)'$ model with an additional gauge singlet scalar particle S .

3.5 Summary

To summarize this section, we have seen that in a simple model with vector mediator, there is a vast range of possibilities for large line signals depending on the nature of the couplings and mass relations. A key-result is that axial couplings are required to have non-vanishing 1-loop cross sections into two gauge bosons. Gamma ray spectra with several lines are typical in the presence of axial couplings. We have presented a minimal anomaly-free construction that realizes non-vanishing axial couplings. It relies on two heavy fermions ψ and ψ' with equal vector couplings and opposite axial couplings to Z' .

If $M_\psi = M_{\psi'}$, the annihilation channels into two gauge bosons, namely into γZ , $\gamma Z'$, ZZ and ZZ' , vanish as the two diagrams with respectively ψ and ψ' in the loop cancel exactly.

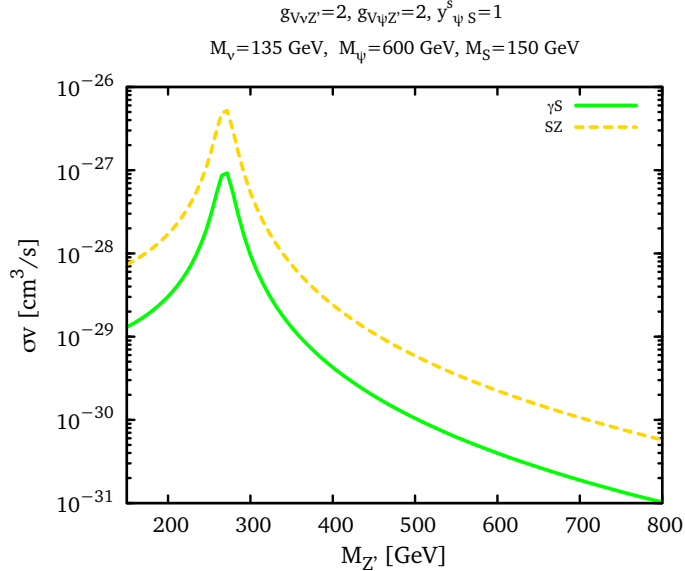


Figure 12: One-loop annihilation cross sections into γS and $Z S$, for the purely vector-like Z' model.

On the other hand, for $\gamma\Phi$ and $Z\Phi$ channels, no such cancellation occurs as these channels do not require axial couplings. In general, M_ψ and $M_{\psi'}$ are different, however there is some partial remnant cancellation which reduces the γZ and $Z Z$ channels relatively to the others. The $\gamma Z'$ and $Z Z'$ channels are not as suppressed (when kinematically allowed) because of the larger couplings involved, $g_{\psi, Z'} \sim 10g_{\psi, Z}$, and two possible axial vertices.

We therefore conclude that quite generally, the $Z\Phi$ and $\gamma\Phi$ channels are the dominant 1-loop annihilation processes.

Similarly to the scalar mediator case, the relic density is complicated and one could imagine several different mechanisms which could arrange for a thermal relic while simultaneously resulting in large gamma ray line signals, but there are no firm generic correlations between the two. Some discussion of the relic density in vector-mediated models can be found in [19].

4 Conclusion

Very large gamma ray line signals would motivate models where DM annihilation rates are enhanced by resonant effects and where the continuum is depressed because of annihilation into heavy channels. In this work we have explored the two main categories which fit easily into the framework of a renormalizable quantum field theory: vector-resonance and scalar-resonance models. We have introduced simple effective field theory sketches of such theories where the dark matter is a Dirac fermion, and performed the first complete analysis which includes the one loop contributions to the continuum annihilation modes.

Both cases, with appropriate choices of couplings, can lead to large line signals as well as large line/continuum ratios. For s -channel vector mediators, this requires chiral couplings to the fermions running in the loop, whereas for scalar mediators, pseudo-scalar couplings with

DM are necessary. The various cases are summarized in tables 1 and 2. We have restricted our models to those in which the fermions running in the loops are disconnected from the SM fermions. We explore the case in which the loop fermions mix with the top quark in a separate publication [19].

Gamma ray lines are a fascinating, powerful probe of dark matter annihilations. Mapping out the kinds of theories which naturally produce such features is an important step in preparing for a discovery.

Acknowledgments

G. Servant is supported by the ERC starting grant Cosmo@LHC (204072). She thanks Sean Tulin for discussions. G. Shaughnessy is supported by the U. S. Department of Energy under the contract DE-FG-02-95ER40896. He also thanks W.-Y. Keung for discussions. T. Tait acknowledges the hospitality of the SLAC theory group, and is supported in part by NSF grant PHY-0970171. He also thanks P. Fox, J. Kearny, and A. Pierce for early collaboration and discussions, and the Aspen Center for Physics, under NSF Grant No. 1066293, where part of this work was completed. The work of M. Taoso is supported by the European Research Council (ERC) under the EU Seventh Framework Programme (FP7/2007-2013) / ERC Starting Grant (agreement n. 278234 - ‘NewDark’ project).

A Effective Vertices and Amplitudes-squared

In the following appendices, we summarize the one-loop expressions for the effective vertices and amplitudes-squared needed for the calculations performed here. The generic topology for the loop diagrams considered here is shown in Fig. 13. We express all amplitudes in terms of two-point (B_0) and three-point (C_0) scalar integrals where:

$$C_0 = C_0(M_1^2, M_2^2, 4M_\nu^2; m_1^2, m_2^2, m_3^2), \quad (12)$$

$$B_0(23) = B_0(M_2^2; m_2^2, m_3^2), \quad (13)$$

$$B_0(13) = B_0(4M_\nu^2; m_1^2, m_3^2), \quad (14)$$

$$B_0(12) = B_0(M_1^2; m_1^2, m_2^2). \quad (15)$$

In the following expressions, for the sake of simplicity, we have set all loop masses equal ($m_1 = m_2 = m_3 \equiv m_f$). However, to derive our results, we have computed all of the expressions in these appendices in terms of the general masses as depicted in Fig. 13.

B One-loop annihilation into $\gamma\gamma$ (and gg)

The annihilation channel $\nu\bar{\nu} \rightarrow \gamma\gamma$ can proceed via s -channel exchange of both a Z' as well as the scalar Φ . The effective vertex for $\Phi(q) \rightarrow \gamma^\mu(p_1)\gamma^\nu(p_2)$ takes the form:

$$\mathcal{V}_{\Phi \rightarrow \gamma\gamma}^{\mu\nu} = Ag^{\mu\nu} + Bp_1^\nu p_2^\mu + iC\epsilon^{p_1 p_2 \nu \mu}, \quad (16)$$

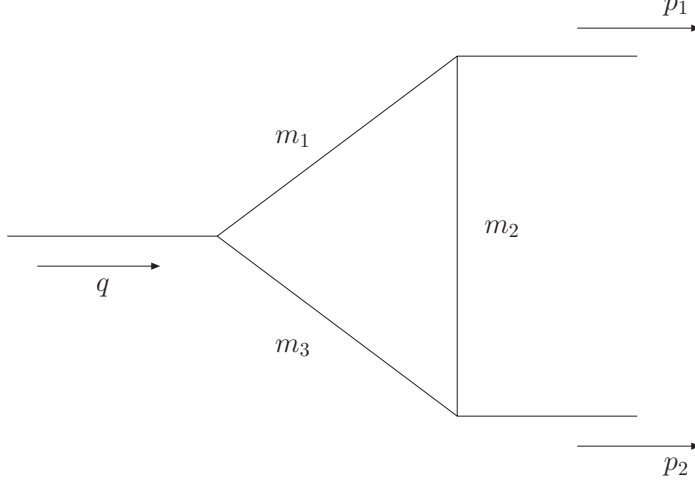


Figure 13: Topology for the effective vertices.

where the coefficients A, B and C are:

$$A = -\frac{v_{(1,2)}^\gamma v_{(2,3)}^\gamma y_{s,(1,3)}^\Phi m_f (2C_0 (m_f^2 - M_\nu^2) + 1)}{2\pi^2} \quad (17)$$

$$B = \frac{v_{(1,2)}^\gamma v_{(2,3)}^\gamma y_{s,(1,3)}^\Phi m_f (2C_0 (m_f^2 - M_\nu^2) + 1)}{4\pi^2 M_\nu^2} \quad (18)$$

$$C = \frac{y_{p,(1,3)}^\Phi v_{(1,2)}^\gamma v_{(2,3)}^\gamma m_f C_0}{2\pi^2} \quad (19)$$

The couplings $y_{s,ff}^\Phi$ and $y_{p,ff}^\Phi$ are the scalar and pseudoscalar couplings, respectively, of Φ to the fermions running in the loop, while $v_{(i,j)}^V$ ($a_{(i,j)}^V$) are the vector (axial-vector) couplings between fermion pair (i, j) and gauge boson V .

The effective vertex for $Z' \rightarrow \gamma\gamma$ can be written as:

$$\mathcal{V}_{Z' \rightarrow \gamma\gamma}^{\alpha\mu\nu} = D \epsilon^{p_1\mu\nu\alpha}, \quad (20)$$

where we have used transversality of the photons (i.e., $\epsilon(p_1) \cdot p_1 = \epsilon(p_2) \cdot p_2 = 0$) as well as the fact that the photons are identical particles to eliminate other possible tensor structures. The loop coefficient D is given by:

$$D = \frac{a_{f\bar{f}}^{Z'}}{4\pi^2} [1 + 2m_f^2 C_0]. \quad (21)$$

Averaging over initial spins, summing over final spins and including a factor of 1/2 for identical particles in the final state, the total matrix-element-squared for $\nu + \bar{\nu} \rightarrow \gamma\gamma$ is given by:

$$\overline{\sum} |\mathcal{M}_{\nu\bar{\nu} \rightarrow \Phi\Phi}|^2 = |\mathcal{M}_\Phi|^2 + |\mathcal{M}_{Z'}|^2 + 2Re |M_\Phi \cdot M_{Z'}^*|, \quad (22)$$

where the matrix-element-squared for the Φ -mediated amplitude is:

$$\overline{\sum} |\mathcal{M}|_{\Phi}^2 = \frac{16 (y_{p,\nu\bar{\nu}}^{\Phi})^2 M_{\nu}^2}{|\Sigma_{\Phi}|^2} [|A|^2 + 4M_{\nu}^4 |C|^2]. \quad (23)$$

The denominator factor Σ_{Φ} is defined as:

$$\Sigma_{\Phi} = 4M_{\nu}^2 - M_{\Phi}^2 + iM_{\Phi}\Gamma_{\Phi}. \quad (24)$$

The amplitude-squared for the Z' -mediated channel is:

$$\overline{\sum} |\mathcal{M}|_{Z'}^2 = \frac{64 (a_{\nu\bar{\nu}}^{Z'})^2 M_{\nu}^4 (4M_{\nu}^2 - M_{Z'}^2)^2}{M_{Z'}^4 |\Sigma_{Z'}|^2} |D|^2, \quad (25)$$

where:

$$\Sigma_{Z'} = 4M_{\nu}^2 - M_{Z'}^2 + iM_{Z'}\Gamma_{Z'}. \quad (26)$$

It is interesting to note that, in the limit where the Z' goes on-shell, we replace $4M_{\nu}^2 \rightarrow M_{Z'}^2$, and the amplitude-squared vanishes as required by the Landau-Yang theorem. The cross term between the Φ - and Z' -mediated processes is given by:

$$2Re |M_{\Phi} \cdot M_{Z'}^*| = -Re \left[\frac{64 y_{p,\nu\bar{\nu}}^{\Phi} a_{\nu\bar{\nu}}^{Z'} M_{\nu}^5 (4M_{\nu}^2 - M_{Z'}^2)}{M_{Z'}^2 \Sigma_{\Phi} \Sigma_{Z'}^*} (CD^* + C^*D) \right], \quad (27)$$

Finally, we note that we can obtain the $\nu\bar{\nu} \rightarrow gg$ channel with the simple rescaling:

$$\sigma_{gg} = \left(\frac{2}{9}\right) \left(\frac{\alpha}{\alpha_s}\right)^2 \frac{1}{Q_t^2} \sigma_{\gamma\gamma}, \quad (28)$$

where Q_t is the charge of the top quark in units of e (i.e., $Q_t = 4/3$).

C One-loop annihilation into $\Phi\Phi$

The annihilation channel $\nu\bar{\nu} \rightarrow \Phi\Phi$ can proceed via both s -channel Φ and Z' exchange. The effective vertex for the $\Phi\Phi\Phi$ vertex takes the form:

$$\mathcal{V}_{\Phi \rightarrow \Phi\Phi} = A \quad (29)$$

where:

$$A = \frac{im_f}{2\pi^2} \left[y_{s,f\bar{f}}^{\Phi} (y_{p,f\bar{f}}^{\Phi})^2 \left(B_0(13) + 2B_0(23) - (2M_{\nu}^2 + M_{\Phi}^2)C_0 \right) - (y_{s,f\bar{f}}^{\Phi})^3 \left(B_0(13) + 2B_0(23) - (2M_{\nu}^2 - 4m_f^2 + M_{\Phi}^2)C_0 \right) \right] \quad (30)$$

while the $Z'\Phi\Phi$ effective vertex is given by:

$$\mathcal{V}_{Z' \rightarrow \Phi\Phi}^{\alpha} = Bp_1^{\alpha} + Cp_2^{\alpha}. \quad (31)$$

The loop coefficients (B and C) in this case are:

$$B = C = -\frac{ia_{ff}^{Z'}y_{p,ff}^\Phi y_{s,ff}^\Phi m_f^2 C_0}{\pi^2}. \quad (32)$$

The amplitude-squared averaged/summed over initial/final spins takes the form:

$$\overline{|\mathcal{M}_{\nu\bar{\nu}\rightarrow\Phi\Phi}|^2} = |\mathcal{M}_\Phi|^2 + |\mathcal{M}_{Z'}|^2 + 2Re|\mathcal{M}_\Phi \cdot \mathcal{M}_{Z'}^*|, \quad (33)$$

where the individual parts are:

$$|\mathcal{M}_\Phi|^2 = \frac{(y_{p,\nu\bar{\nu}}^\Phi)^2 M_\nu^2}{|\Sigma_\Phi|^2} |A|^2, \quad (34)$$

$$\begin{aligned} |\mathcal{M}_{Z'}|^2 &= \frac{1}{M_{Z'}^4 |\Sigma_{Z'}|^2} M_\nu^2 M_{Z'}^4 \left(M_\nu^2 \left((a_{\nu\bar{\nu}}^{Z'})^2 (B+C)(B^*+C^*) \right. \right. \\ &\quad \left. \left. + (v_{\nu\bar{\nu}}^{Z'})^2 (B-C)(B^*-C^*) \right) - (v_{\nu\bar{\nu}}^{Z'})^2 M_\Phi^2 (B-C)(B^*-C^*) \right) \\ &\quad + 16 (a_{\nu\bar{\nu}}^{Z'})^2 M^8 (B+C)(B^*+C^*) \\ &\quad - 8 (a_{\nu\bar{\nu}}^{Z'})^2 M^6 M_{Z'}^2 (B+C)(B^*+C^*), \end{aligned} \quad (35)$$

$$2Re|\mathcal{M}_\Phi \cdot \mathcal{M}_{Z'}^*| = Re \left[\frac{2y_{p,\nu\bar{\nu}}^\Phi v_{\nu\bar{\nu}}^{Z'} M_\nu^3 (4M_\nu^2 - M_{Z'}^2)}{M_{Z'}^2 \Sigma_\Phi \Sigma_{Z'}^*} A (B^* + C^*) \right] \quad (36)$$

Note that a consistent 1-loop calculation of the $\nu\bar{\nu} \rightarrow \Phi\Phi$ channel requires the addition of box diagrams. This is beyond the scope of this paper which is focussed on the topology shown in Fig. 13. In all our illustrative plots, we assume $M_\nu < M_\phi$.

D One-loop annihilation into $V\gamma$

The annihilation $\nu\bar{\nu} \rightarrow V\gamma$ (where $V = Z$ or Z') can proceed via both Φ and Z' s -channel diagrams. The effective vertices take the forms:

$$\mathcal{V}_{\Phi\rightarrow V\gamma}^{\mu\nu} = Ag^{\mu\nu} + Bp_2^\mu p_1^\nu + iC\epsilon^{p_1 p_2 \mu\nu}, \quad (37)$$

and:

$$\mathcal{V}_{Z'\rightarrow V\gamma}^{\alpha\mu\nu} = D\epsilon^{p_1\mu\nu\alpha} + E\epsilon^{p_2\mu\nu\alpha} + Fp_1^\alpha \epsilon^{p_1 p_2 \mu\nu} + Gp_2^\alpha \epsilon^{p_1 p_2 \mu\nu} + Hp_1^\nu \epsilon^{p_1 p_2 \alpha\mu} + Ip_2^\mu \epsilon^{p_1 p_2 \alpha\nu}. \quad (38)$$

The loop coefficients are:

$$A = \frac{v_{ff}^\gamma v_{ff}^V y_{s,ff}^\Phi m_f}{4\pi^2 \left(4M_\nu^2 - M_V^2\right)} \left(M_V^2 \left(-2B_0(13) + 2B_0(23) + C_0 M_V^2 + 4C_0 m_f^2 + 2 \right) \right. \\ \left. + 16C_0 M_\nu^4 - 8M_\nu^2 \left(C_0 \left(M_V^2 + 2m_f^2 \right) + 1 \right) \right), \quad (39)$$

$$B = \frac{v_{ff}^\gamma v_{ff}^V y_{s,ff}^\Phi m_f}{2\pi^2 \left(M_V^2 - 4M_\nu^2 \right)^2} \left(-M_V^2 \left(-2B_0(13) + 2B_0(23) + C_0 M_V^2 + 4C_0 m_f^2 + 2 \right) \right. \\ \left. - 16C_0 M_\nu^4 + 8M_\nu^2 \left(C_0 \left(M_V^2 + 2m_f^2 \right) + 1 \right) \right), \quad (40)$$

$$C = \frac{y_{p,ff}^\Phi v_{ff}^\gamma v_{ff}^V m_f C_0}{2\pi^2}, \quad (41)$$

$$D = \frac{v_{ff}^\gamma}{8\pi^2} \left(\frac{2B_0(12) M_V^2 (a_{ff}^V v_{ff}^{Z'} + a_{ff}^{Z'} v_{ff}^V)}{M_V^2 - 4M_\nu^2} + \frac{B_0(13) \left(4M_\nu^2 + M_V^2\right)^2 (a_{ff}^V v_{ff}^{Z'} + a_{ff}^{Z'} v_{ff}^V)}{\left(M_V^2 - 4M_\nu^2\right)^2} \right. \\ \left. - \frac{2B_0(23) M_V^2 \left(4M_\nu^2 + M_V^2\right) (a_{ff}^V v_{ff}^{Z'} + a_{ff}^{Z'} v_{ff}^V)}{\left(M_V^2 - 4M_\nu^2\right)^2} + 2(B_1(12) + 1) (a_{ff}^V v_{ff}^{Z'} + a_{ff}^{Z'} v_{ff}^V) \right. \\ \left. + 4C_0 m_f^2 (a_{ff}^{Z'} v_{ff}^V - a_{ff}^V v_{ff}^{Z'}) - \frac{8C_0 a_{ff}^V v_{ff}^{Z'} M_\nu^2 M_V^2}{M_V^2 - 4M_\nu^2} - \frac{8C_0 a_{ff}^{Z'} v_{ff}^V M_\nu^2 M_V^2}{M_V^2 - 4M_\nu^2} \right), \quad (42)$$

$$E = -\frac{v_{ff}^\gamma (a_{ff}^V v_{ff}^{Z'} + a_{ff}^{Z'} v_{ff}^V)}{8\pi^2 \left(4M_\nu^2 - M_V^2\right)} \times \\ \left(M_V^2 \left(B_0(13) - B_0(23) - 2C_0 m_f^2 + 1 \right) + M_\nu^2 \left(8C_0 m_f^2 - 4 \right) \right), \quad (43)$$

$$F = -\frac{v_{ff}^\gamma (a_{ff}^V v_{ff}^{Z'} + a_{ff}^{Z'} v_{ff}^V)}{4\pi^2 \left(4M_\nu^2 - M_V^2\right)^3} \left(B_0(13) \left(16M_\nu^4 + 16M_\nu^2 M_V^2 + M_V^4 \right) \right. \\ \left. - 2 \left(M_V^2 \left(4M_\nu^2 \left(B_0(12) + 2B_0(23) + C_0 M_V^2 - 2C_0 m_f^2 - 1 \right) \right) \right. \right. \\ \left. \left. + M_V^2 \left(-B_0(12) + B_0(23) + 2C_0 m_f^2 + 1 \right) - 16C_0 M_\nu^4 \right) \right. \\ \left. - B_1(12) \left(M_V^2 - 4M_\nu^2 \right)^2 \right), \quad (44)$$

$$G = \frac{v_{f\bar{f}}^\gamma (a_{f\bar{f}}^V v_{f\bar{f}}^{Z'} + a_{f\bar{f}}^{Z'} v_{f\bar{f}}^V)}{4\pi^2 (M_V^2 - 4M_\nu^2)} \times \left(M_V^2 (B_0(13) - B_0(23) - 2C_0 m_f^2 - 1) + M_\nu^2 (8C_0 m_f^2 + 4) \right), \quad (45)$$

$$H = -\frac{v_{f\bar{f}}^\gamma (a_{f\bar{f}}^V v_{f\bar{f}}^{Z'} + a_{f\bar{f}}^{Z'} v_{f\bar{f}}^V)}{4\pi^2 (4M_\nu^2 - M_V^2)} \left(-8M_\nu^2 M_V^2 (B_0(12) - 3B_0(13) + 3B_0(23) + 2B_1(12) + C_0 M_V^2 + 2C_0 m_f^2 + 1) + M_V^4 (2B_0(12) - B_0(13) + 2B_1(12)) + 16M_\nu^4 (B_0(13) + 2(B_1(12) + C_0 M_V^2 + 2C_0 m_f^2 + 1)) \right), \quad (46)$$

$$I = \frac{v_{f\bar{f}}^\gamma (a_{f\bar{f}}^V v_{f\bar{f}}^{Z'} + a_{f\bar{f}}^{Z'} v_{f\bar{f}}^V)}{4\pi^2 (M_V^2 - 4M_\nu^2)} \times \left(M_V^2 (B_0(13) - B_0(23) - 2C_0 m_f^2 - 1) + M_\nu^2 (8C_0 m_f^2 + 4) \right) \quad (47)$$

The amplitude-squared averaged/summed over initial/final spins takes the form:

$$\overline{\sum} |\mathcal{M}_{\nu\bar{\nu} \rightarrow V\gamma}|^2 = |\mathcal{M}_\Phi|^2 + |\mathcal{M}_{Z'}|^2 + 2Re |\mathcal{M}_\Phi \cdot \mathcal{M}_{Z'}^*|, \quad (48)$$

where the individual parts are:

$$|\mathcal{M}_\Phi|^2 = \frac{4 (y_{p,\nu\bar{\nu}}^\Phi)^2 M_\nu^2}{|\Sigma_\Phi|^2} \left(4|A|^2 + |C|^2 (M_V^2 - 4M_\nu^2)^2 \right), \quad (49)$$

$$\begin{aligned}
|\mathcal{M}_{Z'}|^2 = & \frac{1}{|\Sigma_{Z'}|^2} \left[\left(v_{\nu\nu}^{Z'} \right)^2 \left(2(DE^* + D^*E) (4M_\nu^2 - M_V^2) (12M_\nu^2 + M_V^2) \right. \right. \\
& + (DF^* + D^*F) (4M_\nu^2 - M_V^2)^3 + (DG^* + D^*G) (M_V^2 - 4M_\nu^2)^3 \\
& + \frac{4(DH^* + D^*H)M_\nu^2 (4M_\nu^2 - M_V^2)^3}{M_V^2} + \frac{|D|^2 (4M_\nu^2 + M_V^2) (M_V^2 - 4M_\nu^2)^2}{M_V^2} \\
& + (EF^* + E^*F) (4M_\nu^2 + M_V^2) (M_V^2 - 4M_\nu^2)^2 \\
& - (EG^* + E^*G) (4M_\nu^2 + M_V^2) (M_V^2 - 4M_\nu^2)^2 + 8(EH^* + E^*H)M_\nu^2 (M_V^2 - 4M_\nu^2)^2 \\
& + |E|^2 (16M_\nu^4 + 24M_\nu^2 M_V^2 + M_V^4) + \frac{1}{2}(FG^* + F^*G) (4M_\nu^2 - M_V^2)^3 (M_V^2 - 4M_\nu^2) \\
& + \frac{1}{4}|F|^2 (M_V^2 - 4M_\nu^2)^4 + \frac{1}{4}|G|^2 (M_V^2 - 4M_\nu^2)^4 + \left. \frac{|H|^2 M_\nu^2 (M_V^2 - 4M_\nu^2)^4}{M_V^2} \right) \\
+ & \left(a_{\nu\nu}^{Z'} \right)^2 \left(-\frac{2(DE^* + D^*E) (4M_\nu^2 - M_V^2)^2 (M_{Z'}^2 - 4M_\nu^2)^2}{M_{Z'}^4} \right. \\
& + \frac{(DF^* + D^*F) (4M_\nu^2 - M_V^2)^3 (M_{Z'}^2 - 4M_\nu^2)^2}{M_{Z'}^4} \\
& + \frac{(DG^* + D^*G) (4M_\nu^2 + M_V^2) (M_V^2 - 4M_\nu^2)^2 (M_{Z'}^2 - 4M_\nu^2)^2}{M_{Z'}^4} \\
& + \frac{|D|^2 (M_V^2 - 4M_\nu^2)^2 (M_{Z'}^2 - 4M_\nu^2)^2}{M_{Z'}^4} \\
& - \frac{(EF^* + E^*F) (4M_\nu^2 - M_V^2) (M_V^2 - 4M_\nu^2)^2 (M_{Z'}^2 - 4M_\nu^2)^2}{M_{Z'}^4} \\
& - \frac{(EG^* + E^*G) (4M_\nu^2 + M_V^2) (M_V^2 - 4M_\nu^2)^2 (M_{Z'}^2 - 4M_\nu^2)^2}{M_{Z'}^4} \\
& + \frac{|E|^2 (M_V^2 - 4M_\nu^2)^2 (M_{Z'}^2 - 4M_\nu^2)^2}{M_{Z'}^4} \\
& + \frac{(FG^* + F^*G) (4M_\nu^2 - M_V^2)^3 (4M_\nu^2 + M_V^2) (M_{Z'}^2 - 4M_\nu^2)^2}{2M_{Z'}^4} \\
& + \frac{|F|^2 (M_V^2 - 4M_\nu^2)^4 (M_{Z'}^2 - 4M_\nu^2)^2}{4M_{Z'}^4} \\
& + \left. \frac{|G|^2 (4M_\nu^2 + M_V^2)^2 (M_V^2 - 4M_\nu^2)^2 (M_{Z'}^2 - 4M_\nu^2)^2}{4M_{Z'}^4} \right) \Bigg],
\end{aligned}$$

$$\begin{aligned}
2\text{Re} |M_\Phi \cdot M_{Z'}^*| = & \text{Re} \left[\frac{a_{\nu\nu}^{Z'} y_{p,\nu\nu}^\Phi M (M_V^2 - 4M^2)^2 (4M^2 - M_{Z'}^2)}{M_{Z'}^2 \Sigma_\Phi \Sigma_{Z'}^*} \times \right. \\
& \left. C (4M^2(F^* + G^*) + M_V^2(G^* - F^*) + 2D^* - 2E^*) \right]. \tag{50}
\end{aligned}$$

E One-loop annihilation into VV

The annihilation channel $\nu\bar{\nu} \rightarrow V_1V_2$ (where possible final states include $ZZ, Z'Z', ZZ'$ and W^+W^-) gets contributions from both s -channel Φ and Z' exchange. The amplitude from the Φ -exchange diagram takes the form:

$$\mathcal{V}_{\Phi \rightarrow V_1V_2}^{\mu\nu} = Ag^{\mu\nu} + Bp_2^\mu p_1^\nu + iC\epsilon^{p_1p_2\mu\nu}, \quad (51)$$

while the effective vertex for the Z' -exchange diagram is given by:

$$\mathcal{V}_{Z' \rightarrow V\gamma}^{\alpha\mu\nu} = D\epsilon^{p_1\mu\nu\alpha} + E\epsilon^{p_2\mu\nu\alpha} + Fp_1^\alpha\epsilon^{p_1p_2\mu\nu} + Gp_2^\alpha\epsilon^{p_1p_2\mu\nu} + Hp_1^\nu\epsilon^{p_1p_2\alpha\mu} + Ip_2^\mu\epsilon^{p_1p_2\alpha\nu}. \quad (52)$$

The loop coefficients for the Φ -exchange diagram are (for simplicity, we assume $V_1 = V_2$):

$$\begin{aligned} A = & -\frac{iy_{s,ff}^{Z'}m_f}{8\pi^2(M_\nu^2 - M_V^2)} \left(\left(a_{f\bar{f}}^V \right)^2 \left(M_V^2 \left(3B_0(12) + 2B_0(13) + 3B_0(23) - 2C_0M_V^2 \right. \right. \right. \\ & \left. \left. \left. + 8C_0m_f^2 - 4 \right) - 4M_\nu^2 (B_0(12) + B_0(23) + C_0M_V^2 + 2C_0m_f^2 - 1) + 8C_0M_\nu^4 \right) \right. \\ & \left. + \left(v_{f\bar{f}}^V \right)^2 \left(-M_V^2 (B_0(12) - 2B_0(13) + B_0(23) + 2C_0M_V^2 + 8C_0m_f^2 + 4) \right. \right. \\ & \left. \left. - 8C_0M_\nu^4 + 4M_\nu^2 (3C_0M_V^2 + 2C_0m_f^2 + 1) \right) \right), \quad (53) \end{aligned}$$

$$\begin{aligned} B = & \frac{iy_{s,ff}^{Z'}m_f}{16\pi^2M^2(M^2 - M_V^2)^2} \left(\left(a_{f\bar{f}}^V \right)^2 (2M^2 - M_V^2) \left(M^2 \left(4B_0(13) - 4B_0(23) - 2C_0M_V^2 \right. \right. \right. \\ & \left. \left. \left. + 4C_0m_f^2 + 2 \right) + M_V^2 (-B_0(13) + B_0(23) + C_0M_V^2 - 4C_0m_f^2 - 2) + 4C_0M^4 \right) \right. \\ & \left. + \left(v_{f\bar{f}}^V \right)^2 \left(-2M^2M_V^2 (-B_0(13) + B_0(23) + 2C_0M_V^2 + 6C_0m_f^2 + 3) \right. \right. \\ & \left. \left. + M_V^4 (B_0(13) - B_0(23) - C_0M_V^2 + 4C_0m_f^2 + 2) - 8C_0M^6 \right. \right. \\ & \left. \left. + 4M^4 (2C_0 (2M_V^2 + m_f^2) + 1) \right) \right), \quad (54) \end{aligned}$$

$$\begin{aligned} C = & -\frac{y_{p,ff}^{Z'}m_f}{2\pi^2(M - M_V)(M + M_V)} \left(B_0(13) \left(a_{f\bar{f}}^V \right)^2 - B_0(23) \left(a_{f\bar{f}}^V \right)^2 \right. \\ & \left. + C_0M^2 (a_{f\bar{f}}^V - v_{f\bar{f}}^V)(a_{f\bar{f}}^V + v_{f\bar{f}}^V) + C_0 \left(v_{f\bar{f}}^V \right)^2 M_V^2 \right), \quad (55) \end{aligned}$$

while the loop coefficients for the Z' -exchange diagram are:

$$D = \frac{1}{4\pi^2} \left(a_{ff}^{Z'} \left((a_{ff}^V)^2 + (v_{ff}^V)^2 \right) + 2a_{ff}^V v_{ff}^V v_{ff}^{Z'} \right) - 2a_{ff}^{Z'} m_f^2 \left(B_0(13) (a_{ff}^V)^2 - B_0(23) (a_{ff}^V)^2 + C_0 M_\nu^2 (a_{ff}^V - v_{ff}^V) (a_{ff}^V + v_{ff}^V) + C_0 (v_{ff}^V)^2 M_V^2 \right), \quad (56)$$

$$E = \frac{2a_{ff}^{Z'} m_f^2}{4\pi^2 (M_\nu^2 - M_V^2)} \left(B_0(13) (a_{ff}^V)^2 - B_0(23) (a_{ff}^V)^2 + C_0 M_\nu^2 (a_{ff}^V - v_{ff}^V) (a_{ff}^V + v_{ff}^V) + C_0 (v_{ff}^V)^2 M_V^2 \right) - (M_\nu - M_V) (M_\nu + M_V) \left(a_{ff}^{Z'} \left((a_{ff}^V)^2 + (v_{ff}^V)^2 \right) + 2a_{ff}^V v_{ff}^V v_{ff}^{Z'} \right), \quad (57)$$

$$F = 0, \quad (58)$$

$$G = 0, \quad (59)$$

$$H = -\frac{\left(a_{ff}^{Z'} \left((a_{ff}^V)^2 + (v_{ff}^V)^2 \right) + 2a_{ff}^V v_{ff}^V v_{ff}^{Z'} \right)}{32\pi^2 M_\nu^2 (M_\nu^2 - M_V^2)^2} \left(2M_\nu^2 M_V^2 \left(B_0(13) - B_0(23) + 2C_0 M_V^2 - 6C_0 m_f^2 - 3 \right) + M_V^4 \left(B_0(13) - B_0(23) - C_0 M_V^2 + 4C_0 m_f^2 + 2 \right) + M_\nu^4 \left(8C_0 m_f^2 + 4 \right) \right), \quad (60)$$

$$I = \frac{\left(a_{ff}^{Z'} \left((a_{ff}^V)^2 + (v_{ff}^V)^2 \right) + 2a_{ff}^V v_{ff}^V v_{ff}^{Z'} \right)}{32\pi^2 M_\nu^2 (M_\nu^2 - M_V^2)^2} \left(2M_\nu^2 M_V^2 \left(B_0(13) - B_0(23) + 2C_0 M_V^2 - 6C_0 m_f^2 - 3 \right) + M_V^4 \left(B_0(13) - B_0(23) - C_0 M_V^2 + 4C_0 m_f^2 + 2 \right) + M_\nu^4 \left(8C_0 m_f^2 + 4 \right) \right). \quad (61)$$

The contributions to the total amplitude-squared are:

$$|\mathcal{M}_\Phi|^2 = \frac{8(y_{p,\nu\bar{\nu}}^\Phi)^2 M^2}{M_V^4 |\Sigma_\Phi|^2} \left(8M^2 (M - M_V) (M + M_V) \left(-M_V^2 ((AB^* + A^*B) + 2|B|^2 M^2) + 2(AB^* + A^*B)M^2 + 2|B|^2 M^4 + |C|^2 M_V^4 \right) + |A|^2 (4M^4 - 4M^2 M_V^2 + 3M_V^4) \right), \quad (62)$$

$$\begin{aligned}
|\mathcal{M}_{Z'}|^2 &= \frac{16}{M_V^2 M_{Z'}^4 |\Gamma_{Z'}|^2} \left(M_\nu^2 M_{Z'}^4 \left(M_V^4 \left(\left(a_{\nu\bar{\nu}}^{Z'} \right)^2 - 2 \left(v_{\nu\bar{\nu}}^{Z'} \right)^2 \right) \left(2(DE^* + D^*E) \right. \right. \right. \\
&\quad \left. \left. - |D|^2 - |E|^2 \right) + 8 \left(v_{\nu\bar{\nu}}^{Z'} \right)^2 M_\nu^2 \left((DH^* + D^*H) - (DI^* + D^*I) \right. \right. \\
&\quad \left. \left. - (EH^* + E^*H) + (EI^* + E^*I) \right) + 16 \left(v_{\nu\bar{\nu}}^{Z'} \right)^2 M_\nu^4 (|H|^2 + |I|^2) \right) \\
&\quad + M_\nu^2 M_V^2 \left(-2(DE^* + D^*E) \left(\left(a_{\nu\bar{\nu}}^{Z'} \right)^2 - 5 \left(v_{\nu\bar{\nu}}^{Z'} \right)^2 \right) \right. \\
&\quad \left. + 8 \left(v_{\nu\bar{\nu}}^{Z'} \right)^2 M_\nu^2 \left(-3(DH^* + D^*H) + (DI^* + D^*I) + (EH^* + E^*H) \right. \right. \\
&\quad \left. \left. - 3(EI^* + E^*I) \right) + (|D|^2 + |E|^2) \left(\left(a_{\nu\bar{\nu}}^{Z'} \right)^2 - 3 \left(v_{\nu\bar{\nu}}^{Z'} \right)^2 \right) \right. \\
&\quad \left. - 32 \left(v_{\nu\bar{\nu}}^{Z'} \right)^2 M_\nu^4 (|H|^2 + |I|^2) \right) + 4 \left(v_{\nu\bar{\nu}}^{Z'} \right)^2 M_\nu^4 \left(4M_\nu^2 \left((DH^* + D^*H) \right. \right. \\
&\quad \left. \left. + (EI^* + E^*I) + M_\nu^2 (|H|^2 + |I|^2) \right) + |D|^2 + |E|^2 \right) \\
&\quad + 16 \left(a_{\nu\bar{\nu}}^{Z'} \right)^2 M_\nu^6 M_V^2 (M_\nu - M_V)(M_\nu + M_V) (-2(DE^* + D^*E) + |D|^2 + |E|^2) \\
&\quad - 8 \left(a_{\nu\bar{\nu}}^{Z'} \right)^2 M_\nu^4 M_V^2 M_{Z'}^2 (M_\nu - M_V)(M_\nu + M_V) (-2(DE^* + D^*E) \\
&\quad \left. + |D|^2 + |E|^2) \right) \tag{63}
\end{aligned}$$

$$2Re |M_\Phi \cdot M_{Z'}^*| = Re \left[\frac{32 a_{\nu\bar{\nu}}^{Z'} y_{p,\nu\bar{\nu}}^\Phi M_\nu^3 C (M_\nu^2 - M_V^2) (4M_\nu^2 - M_{Z'}^2) (D^* - E^*)}{M_{Z'}^2 \Gamma_\Phi (\Gamma_{Z'})^*} \right] \tag{64}$$

F One-loop annihilation into $\gamma\Phi$

The annihilation mode $\nu\bar{\nu} \rightarrow \gamma\Phi$ can only proceed via s -channel Z' exchange. The effective vertex for the $Z'\gamma\Phi$ interaction takes the form:

$$\mathcal{V}_{Z' \rightarrow \gamma\Phi}^{\alpha\mu} = Ag^{\alpha\mu} + iB\epsilon^{p_1 p_2 \alpha\mu}, \tag{65}$$

where the loop coefficients are:

$$\begin{aligned}
A &= -\frac{v_{f\bar{f}}^\gamma y_{s,f\bar{f}}^\Phi v_{f\bar{f}}^{Z'} m_f}{4\pi^2 \left(4M_\nu^2 - M_\Phi^2 \right)} \left(8M_\nu^2 \left(B_0(13) - B_0(23) - C_0 M_\Phi^2 + 2C_0 m_f^2 + 1 \right) \right. \\
&\quad \left. + 16C_0 M_\nu^4 + M_\Phi^2 \left(C_0 \left(M_\Phi^2 - 4m_f^2 \right) - 2 \right) \right), \tag{66}
\end{aligned}$$

$$B = -\frac{v_{f\bar{f}}^\gamma y_{p,f\bar{f}}^\Phi v_{f\bar{f}}^{Z'} m_f C_0}{2\pi^2}. \tag{67}$$

The amplitude-squared is:

$$|\mathcal{M}|^2 = \frac{v_{\nu\bar{\nu}}^2}{4|\Sigma_{Z'}|^2} \left[4|A|^2 + (4M_\nu^2 - M_\Phi^2)^2 |B|^2 \right] \quad (68)$$

G One-loop annihilation into $V\Phi$

As for the $\gamma\Phi$ channel, the annihilation into $V\Phi$ (where $V = Z, Z'$) can only proceed via an s -channel Z' . The effective vertex is given by:

$$\mathcal{V}_{Z' \rightarrow V\Phi}^{\alpha\mu} = Ag^{\alpha\mu} + Bp_1^\alpha p_2^\mu + Cp_1^\alpha p_2^\mu + iD\epsilon^{p_1 p_2 \mu\alpha}. \quad (69)$$

The loop coefficients for this process are:

$$\begin{aligned} A = & -\frac{v_{f\bar{f}}^V m_f}{4\pi^2 \left(-2M_\Phi^2 \left(4M_\nu^2 + M_V^2 \right) + \left(M_V^2 - 4M_\nu^2 \right)^2 + M_\Phi^4 \right)} \times \\ & \left(y_{p,f\bar{f}}^\Phi \alpha_{f\bar{f}}^{Z'} \left(-4M_\nu^2 \left(-2M_V^2 \left(B_0(12) + B_0(13) + 2B_0(23) - C_0 M_\Phi^2 + 4C_0 m_f^2 - 2 \right) \right. \right. \right. \\ & \left. \left. \left. + M_\Phi^2 \left(-4B_0(12) - 2B_0(13) - 2B_0(23) + C_0 M_\Phi^2 - 8C_0 m_f^2 + 4 \right) + C_0 M_V^4 \right) \right. \right. \\ & \left. \left. + (M_V - M_\Phi)(M_V + M_\Phi) \left(M_\Phi^2 \left(2B_0(12) + 2B_0(13) - C_0 M_\Phi^2 + 4C_0 m_f^2 - 2 \right) \right. \right. \right. \\ & \left. \left. \left. - 2M_V^2 \left(B_0(13) + B_0(23) + 2C_0 m_f^2 - 1 \right) + C_0 M_V^4 \right) - 16M_\nu^4 \left(2B_0(12) + 2B_0(23) \right. \right. \right. \\ & \left. \left. \left. + C_0 \left(M_V^2 + M_\Phi^2 + 4m_f^2 \right) - 2 \right) + 64C_0 M_\nu^6 \right) + y_{s,f\bar{f}}^\Phi v_{f\bar{f}}^{Z'} \left(-4M_\nu^2 \left(2M_V^2 \left(B_0(12) \right. \right. \right. \right. \\ & \left. \left. \left. + B_0(13) - 2B_0(23) - C_0 M_\Phi^2 + 4C_0 m_f^2 + 2 \right) + M_\Phi^2 \left(2B_0(13) - 2B_0(23) - 3C_0 M_\Phi^2 \right. \right. \right. \\ & \left. \left. \left. + 8C_0 m_f^2 + 4 \right) + C_0 M_V^4 \right) + (M_V - M_\Phi)(M_V + M_\Phi) \left(2M_V^2 \left(B_0(12) - B_0(23) \right. \right. \right. \\ & \left. \left. \left. - C_0 M_\Phi^2 + 2C_0 m_f^2 + 1 \right) + C_0 M_V^4 + M_\Phi^2 \left(C_0 M_\Phi^2 - 4C_0 m_f^2 - 2 \right) \right) \right) \\ & \left. \left. \left. + 16M_\nu^4 \left(2B_0(13) - 2B_0(23) - C_0 \left(M_V^2 + 3M_\Phi^2 - 4m_f^2 \right) + 2 \right) + 64C_0 M_\nu^6 \right) \right), \quad (70) \end{aligned}$$

$$\begin{aligned}
B = & - \frac{a_{f\bar{f}}^V M_V^2 m_f (y_{p,f\bar{f}}^\Phi a_{f\bar{f}}^{Z'} + y_{s,f\bar{f}}^\Phi v_{f\bar{f}}^{Z'})}{\pi^2 \left(-2M_\Phi^2 (4M_\nu^2 + M_V^2) + (M_V^2 - 4M_\nu^2)^2 + M_\Phi^4 \right)^2} \times \\
& \left(-16M_\nu^4 (2B_0(12) - 4B_0(13) + 2B_0(23) + C_0 (M_V^2 + M_\Phi^2 - 4m_f^2) - 2) \right. \\
& - 4M_\nu^2 \left(2M_V^2 (B_0(12) + B_0(13) - 2B_0(23) - 3C_0 M_\Phi^2 + 4C_0 m_f^2 + 2) \right. \\
& + M_\Phi^2 (-4B_0(12) + 2B_0(13) + 2B_0(23) + C_0 M_\Phi^2 + 8C_0 m_f^2 + 4) + C_0 M_V^4 \left. \right) \\
& + (M_V - M_\Phi)(M_V + M_\Phi) \left(M_V^2 (4B_0(12) - 2B_0(13) - 2B_0(23) + 4C_0 m_f^2 + 2) \right. \\
& - M_\Phi^2 (-2B_0(12) - 2B_0(13) + 4B_0(23) + C_0 M_\Phi^2 + 4C_0 m_f^2 + 2) + C_0 M_V^4 \left. \right) \\
& \left. + 64C_0 M_\nu^6 \right), \tag{71}
\end{aligned}$$

$$\begin{aligned}
C = & \frac{v_{f\bar{f}}^V m_f}{2\pi^2(2M_\nu - M_V + M_\Phi)^2(2M_\nu + M_V + M_\Phi)^2 \left(M_V^2 - (M_\Phi - 2M)^2 \right)^2} \times \\
& \left(y_{p,f\bar{f}}^\Phi a_{f\bar{f}}^{Z'} \left(4M_\nu^2 - M_V^2 - M_\Phi^2 \right) \left(-16M_\nu^4 \left(2B_0(12) - 4B_0(13) + 2B_0(23) \right) \right. \right. \\
& + C_0 \left(M_V^2 + M_\Phi^2 - 4m_f^2 \right) - 2 \left. \right) - 4M_\nu^2 \left(2M_V^2 \left(B_0(12) + B_0(13) - 2B_0(23) \right) \right. \\
& - 3C_0 M_\Phi^2 + 4C_0 m_f^2 + 2 \left. \right) + M_\Phi^2 \left(-4B_0(12) + 2B_0(13) + 2B_0(23) + C_0 M_\Phi^2 + 8C_0 m_f^2 + 4 \right) \\
& + C_0 M_V^4 \left. \right) + (M_V - M_\Phi)(M_V + M_\Phi) \left(M_V^2 \left(4B_0(12) - 2B_0(13) - 2B_0(23) + 4C_0 m_f^2 + 2 \right) \right. \\
& - M_\Phi^2 \left(-2B_0(12) - 2B_0(13) + 4B_0(23) + C_0 M_\Phi^2 + 4C_0 m_f^2 + 2 \right) + C_0 M_V^4 \left. \right) + 64C_0 M_\nu^6 \left. \right) \\
+ & y_{s,f\bar{f}}^\Phi v_{f\bar{f}}^{Z'} \left(-32M_\nu^4 \left(M_V^2 \left(3B_0(12) - 3B_0(23) - 5C_0 M_\Phi^2 + 6C_0 m_f^2 + 3 \right) + M_\Phi^2 \left(2B_0(13) \right. \right. \right. \\
& - 2B_0(23) - 3C_0 M_\Phi^2 + 6C_0 m_f^2 + 3 \left. \left. \right) \right) + 8M_\nu^2 \left(M_V^4 \left(6B_0(12) - 3B_0(13) - 3B_0(23) \right. \right. \\
& - 2C_0 M_\Phi^2 + 6C_0 m_f^2 + 3 \left. \left. \right) + M_V^2 M_\Phi^2 \left(6B_0(13) - 6B_0(23) - C_0 M_\Phi^2 + 4C_0 m_f^2 + 2 \right) \right. \\
& + M_\Phi^4 \left(B_0(13) - B_0(23) - 2C_0 M_\Phi^2 + 6C_0 m_f^2 + 3 \right) + C_0 M_V^6 \left. \right) \\
& - (M_V - M_\Phi)(M_V + M_\Phi) \left(M_V^4 \left(6B_0(12) - 4B_0(13) - 2B_0(23) + 3C_0 M_\Phi^2 + 4C_0 m_f^2 + 2 \right) \right. \\
& + M_V^2 M_\Phi^2 \left(6B_0(12) + 4B_0(13) - 10B_0(23) - 5C_0 M_\Phi^2 \right) + C_0 M_V^6 + M_\Phi^4 \left(C_0 M_\Phi^2 - 4C_0 m_f^2 \right. \\
& \left. \left. - 2 \right) \right) + 128M_\nu^6 \left(B_0(13) - B_0(23) - C_0 \left(M_V^2 + 2M_\Phi^2 - 2m_f^2 \right) + 1 \right) + 256C_0 M_\nu^8 \left. \right), \quad (72)
\end{aligned}$$

$$\begin{aligned}
D = & - \frac{a_{f\bar{f}}^V m_f}{2\pi^2 \left(-2M_\Phi^2 \left(4M_\nu^2 + M_V^2 \right) + \left(M_V^2 - 4M_\nu^2 \right)^2 + M_\Phi^4 \right)} \times \\
& \left(2M_\Phi^2 \left(y_{p,f\bar{f}}^\Phi a_{f\bar{f}}^{Z'} (B_0(12) + B_0(13) - 2B_0(23)) - C_0 y_{s,f\bar{f}}^\Phi v_{f\bar{f}}^{Z'} \left(4M_\nu^2 + M_V^2 \right) \right) \right. \\
& + \left(4M_\nu^2 - M_V^2 \right) \left(-2B_0(12) y_{p,f\bar{f}}^\Phi a_{f\bar{f}}^{Z'} + 2B_0(13) y_{p,f\bar{f}}^\Phi a_{f\bar{f}}^{Z'} \right. \\
& \left. \left. + C_0 \left(4M_\nu^2 - M_V^2 \right) \left(y_{p,f\bar{f}}^\Phi a_{f\bar{f}}^{Z'} + y_{s,f\bar{f}}^\Phi v_{f\bar{f}}^{Z'} \right) + C_0 M_\Phi^4 \left(y_{s,f\bar{f}}^\Phi v_{f\bar{f}}^{Z'} - y_{p,f\bar{f}}^\Phi a_{f\bar{f}}^{Z'} \right) \right) \quad (73)
\end{aligned}$$

Finally, the matrix-element-squared is given by:

$$\begin{aligned}
|\mathcal{M}|^2 = & \frac{1}{|\Sigma_{Z'}|^2} \left[\frac{(AB^* + A^*B)}{16M_V^2 M_{Z'}^4} \left(-2M_\Phi^2 (4M^2 + M_V^2) + (M_V^2 - 4M^2)^2 + M_\Phi^4 \right) \times \right. \\
& \left((a_{\nu\nu}^{Z'})^2 (M_{Z'}^2 - 4M^2)^2 (4M^2 - M_V^2 + M_\Phi^2) + (v_{\nu\nu}^{Z'})^2 M_{Z'}^4 (-4M^2 - M_V^2 + M_\Phi^2) \right) \\
& + \frac{(AC^* + A^*C)}{16M_V^2 M_{Z'}^4} (-2M_\nu + M_V - M_\Phi)(2M_\nu + M_V - M_\Phi)(-2M_\nu + M_V + M_\Phi) \times \\
& (2M_\nu + M_V + M_\Phi) (4M^2 + M_V^2 - M_\Phi^2) \left((a_{\nu\nu}^{Z'})^2 (M_{Z'}^2 - 4M^2)^2 \right. \\
& \left. + (v_{\nu\nu}^{Z'})^2 M_{Z'}^4 \right) 16M_V^2 M_{Z'}^4 \\
& + \frac{|A|^2}{8M_V^2 M_{Z'}^4} \left((a_{\nu\nu}^{Z'})^2 (M_{Z'}^2 - 4M^2)^2 \left(-2M_\Phi^2 (4M^2 + M_V^2) + (M_V^2 - 4M^2)^2 + M_\Phi^4 \right) \right. \\
& \left. + (v_{\nu\nu}^{Z'})^2 M_{Z'}^4 \left(16M^4 + 8M^2 (5M_V^2 - M_\Phi^2) + (M_V^2 - M_\Phi^2)^2 \right) \right) \\
& + \frac{(BC^* + B^*C)}{32M_V^2 M_{Z'}^4} \left(-2M_\Phi^2 (4M^2 + M_V^2) + (M_V^2 - 4M^2)^2 + M_\Phi^4 \right) \times \\
& \left((a_{\nu\nu}^{Z'})^2 (M_{Z'}^2 - 4M^2)^2 \left(16M^4 - (M_V^2 - M_\Phi^2)^2 \right) \right. \\
& \left. - (v_{\nu\nu}^{Z'})^2 M_{Z'}^4 \left(-2M_\Phi^2 (4M^2 + M_V^2) + (M_V^2 - 4M^2)^2 + M_\Phi^4 \right) \right) \\
& + \frac{|B|^2}{32M_V^2 M_{Z'}^4} \left(-2M_\Phi^2 (4M^2 + M_V^2) + (M_V^2 - 4M^2)^2 + M_\Phi^4 \right) \times \\
& \left((a_{\nu\nu}^{Z'})^2 (M_{Z'}^2 - 4M^2)^2 (4M^2 - M_V^2 + M_\Phi^2)^2 \right. \\
& \left. + (v_{\nu\nu}^{Z'})^2 M_{Z'}^4 \left(-2M_\Phi^2 (4M^2 + M_V^2) + (M_V^2 - 4M^2)^2 + M_\Phi^4 \right) \right) \\
& + \frac{|C|^2}{32M_V^2 M_{Z'}^4} \left(-2M_\Phi^2 (4M^2 + M_V^2) + (M_V^2 - 4M^2)^2 + M_\Phi^4 \right) \times \\
& \left((a_{\nu\nu}^{Z'})^2 (M_{Z'}^2 - 4M^2)^2 (4M^2 + M_V^2 - M_\Phi^2)^2 \right. \\
& \left. + (v_{\nu\nu}^{Z'})^2 M_{Z'}^4 \left(-2M_\Phi^2 (4M^2 + M_V^2) + (M_V^2 - 4M^2)^2 + M_\Phi^4 \right) \right) \\
& \left. + |D|^2 (v_{\nu\nu}^{Z'})^2 M^2 \left(-2M_\Phi^2 (4M^2 + M_V^2) + (M_V^2 - 4M^2)^2 + M_\Phi^4 \right) \right]. \tag{74}
\end{aligned}$$

References

- [1] M. Ackermann *et al.* [Fermi-LAT Collaboration], Phys. Rev. Lett. **107**, 241302 (2011) [arXiv:1108.3546 [astro-ph.HE]].
- [2] M. Ackermann *et al.* [LAT Collaboration], Phys. Rev. D **86**, 022002 (2012) [arXiv:1205.2739 [astro-ph.HE]].
- [3] C. B. Jackson, G. Servant, G. Shaughnessy, T. M. P. Tait and M. Taoso, JCAP **1004**, 004 (2010) [arXiv:0912.0004 [hep-ph]].
- [4] B. Lillie, J. Shu and T. M. P. Tait, JHEP **0804**, 087 (2008) [arXiv:0712.3057 [hep-ph]].
- [5] K. Kumar, T. M. P. Tait and R. Vega-Morales, JHEP **0905**, 022 (2009) [arXiv:0901.3808 [hep-ph]].
- [6] A. Pomarol and J. Serra, Phys. Rev. D **78**, 074026 (2008) [arXiv:0806.3247 [hep-ph]].
- [7] K. Agashe and G. Servant, JCAP **0502**, 002 (2005) [hep-ph/0411254].
- [8] E. Dudas, Y. Mambrini, S. Pokorski and A. Romagnoni, JHEP **0908**, 014 (2009) [arXiv:0904.1745 [hep-ph]]; Y. Mambrini, JCAP **0912**, 005 (2009) [arXiv:0907.2918 [hep-ph]]; E. Dudas, Y. Mambrini, S. Pokorski and A. Romagnoni, arXiv:1205.1520 [hep-ph]; M. R. Buckley and D. Hooper, Phys. Rev. D **86**, 043524 (2012) [arXiv:1205.6811 [hep-ph]]; Z. Kang, T. Li, J. Li and Y. Liu, arXiv:1206.2863 [hep-ph]; S. Tulin, H. -B. Yu and K. M. Zurek, arXiv:1208.0009 [hep-ph]; Y. Bai and J. Shelton, JHEP **1212**, 056 (2012) [arXiv:1208.4100 [hep-ph]]; H. M. Lee, M. Park and W. -I. Park, JHEP **1212**, 037 (2012) [arXiv:1209.1955 [hep-ph]]; N. Bernal, C. Boehm, S. Palomares-Ruiz, J. Silk and T. Toma, arXiv:1211.2639 [hep-ph]; H. M. Lee, M. Park and V. Sanz, arXiv:1212.5647 [hep-ph]; J. Kopp, E. T. Neil, R. Primulando and J. Zupan, arXiv:1301.1683 [hep-ph]; J. Fan and M. Reece, arXiv:1301.2597 [hep-ph].
- [9] T. Cohen, M. Lisanti, T. R. Slatyer and J. G. Wacker, JHEP **1210**, 134 (2012) [arXiv:1207.0800 [hep-ph]].
- [10] G. Bertone, C. B. Jackson, G. Shaughnessy, T. M. P. Tait and A. Vallinotto, Phys. Rev. D **80**, 023512 (2009) [arXiv:0904.1442 [astro-ph.HE]].
- [11] A. Rajaraman, T. M. P. Tait and D. Whiteson, JCAP **1209**, 003 (2012) [arXiv:1205.4723 [hep-ph]]; A. Rajaraman, T. M. P. Tait and A. M. Wijangco, arXiv:1211.7061 [hep-ph].
- [12] T. Bringmann, X. Huang, A. Ibarra, S. Vogl and C. Weniger, JCAP **1207**, 054 (2012) [arXiv:1203.1312 [hep-ph]]; C. Weniger, JCAP **1208**, 007 (2012) [arXiv:1204.2797 [hep-ph]]; A. Hektor, M. Raidal and E. Tempel, Astrophys. J. **762**, L22 (2013) [arXiv:1207.4466 [astro-ph.HE]]; M. Su and D. P. Finkbeiner, arXiv:1206.1616 [astro-ph.HE].
- [13] D. Whiteson, JCAP **1211**, 008 (2012) [arXiv:1208.3677 [astro-ph.HE]]; D. P. Finkbeiner, M. Su and C. Weniger, JCAP **1301**, 029 (2013) [arXiv:1209.4562 [astro-ph.HE]]; A. Hektor, M. Raidal and E. Tempel, arXiv:1209.4548 [astro-ph.HE].

- [14] M. E. Peskin and T. Takeuchi, Phys. Rev. D **46**, 381 (1992).
- [15] X. Chu, T. Hambye, T. Scarna and M. H. G. Tytgat, Phys. Rev. D **86**, 083521 (2012) [arXiv:1206.2279 [hep-ph]].
- [16] Y. Zhang, arXiv:1212.2730 [hep-ph].
- [17] K. Rao and D. Whiteson, arXiv:1204.4504 [hep-ph].
- [18] S. Chatrchyan *et al.* [CMS Collaboration], arXiv:1203.5410 [hep-ex].
- [19] C. B. Jackson, G. Servant, G. Shaughnessy, T. M. P. Tait and M. Taoso, arXiv:1303.4717 [hep-ph].
- [20] L. D. Landau, Dokl. Akad. Nauk., USSR **60**, 207 (1948); C. N. Yang, Phys. Rev. **77**, 242 (1950).
- [21] J. R. Espinosa, B. Gripaios, T. Konstandin and F. Riva, JCAP **1201**, 012 (2012) [arXiv:1110.2876 [hep-ph]].
- [22] B. Gripaios, A. Pomarol, F. Riva and J. Serra, JHEP **0904**, 070 (2009) [arXiv:0902.1483 [hep-ph]].